NeuroImage 245 (2021) 118651

Contents lists available at ScienceDirect

NeuroImage

journal homepage: www.elsevier.com/locate/neuroimage

Tractography methods and findings in brain tumors and traumatic brain injury

Fang-Cheng Yeh[a,b,*], Andrei Irimia[c,d], Dhiego Chaves de Almeida Bastos[e], Alexandra J. Golby[e,f]

[a] Department of Neurological Surgery, University of Pittsburgh Medical Center, Pittsburgh, Pennsylvania, USA
[b] Department of Bioengineering, University of Pittsburgh, Pittsburgh, Pennsylvania, USA
[c] Ethel Percy Andrus Gerontology Center, Leonard Davis School of Gerontology, University of Southern California, Los Angeles, California, USA
[d] Corwin D. Denney Research Center, Department of Biomedical Engineering, Viterbi School of Engineering, University of Southern California, Los Angeles, California, USA
[e] Department of Neurosurgery, Brigham and Women's Hospital, Harvard Medical School, Boston, Massachusetts, USA
[f] Department of Radiology, Brigham and Women's Hospital, Harvard Medical School, Boston, Massachusetts, USA

ARTICLE INFO

Keywords:
Diffusion MRI
fiber tracking
tractography
brain tumor
glioma
traumatic brain injury

ABSTRACT

White matter fiber tracking using diffusion magnetic resonance imaging (dMRI) provides a noninvasive approach to map brain connections, but improving anatomical accuracy has been a significant challenge since the birth of tractography methods. Utilizing tractography in brain studies therefore requires understanding of its technical limitations to avoid shortcomings and pitfalls. This review explores tractography limitations and how different white matter pathways pose different challenges to fiber tracking methodologies. We summarize the pros and cons of commonly-used methods, aiming to inform how tractography and its related analysis may lead to questionable results. Extending these experiences, we review the clinical utilization of tractography in patients with brain tumors and traumatic brain injury, starting from tensor-based tractography to more advanced methods. We discuss current limitations and highlight novel approaches in the context of these two conditions to inform future tractography developments.

1. Introduction

Diffusion magnetic resonance imaging (dMRI) fiber tracking (Basser et al., 2000; Mori et al., 1999) has been available to the neuroscience community for two decades and remains the only non-invasive way to systematically map white matter tracts in the human brain (Craddock et al., 2013). Since their inception, fiber tracking approaches have been leveraged as powerful tools to understand the circuit mechanisms behind normal and abnormal brain functions (Behrens et al., 2003a; Schmahmann et al., 2007). The region-to-region connectivity mapped by tractography facilitates the inference of the *structural connectome* to elucidate brain network topology (Sporns et al., 2005) and inform how brain connectivity patterns contribute to brain functions. Although widely used in neuroscience research, fiber tracking has yet to acquire widespread clinical utility for neurological disorders. The primary limitation against such a more comprehensive application is that utilizing and interpreting tractography requires a substantial understanding of brain architecture (Schilling et al., 2020) and the tractography method (O'Donnell and Pasternak, 2014). These factors are essential because tractography can yield false positive and false negative results (Kupper et al., 2015; Maier-Hein et al., 2017; Thomas et al., 2014).

The purpose of this review is to provide background for an audience with neuroimaging backgrounds aiming to acquire essential knowledge on tractography to investigate brain conditions involving gross pathologies, such as brain tumors and traumatic brain injuries (TBIs). Sections are presented in the following order to provide the information we deem essential. First, with histology images, we highlight the challenges of fiber tracking in various brain regions. Second, we provide an overview of dMRI acquisition, modeling methods, and fiber tracking algorithms and discuss their relative strengths and weaknesses. Instead of providing a glimpse into all methods, we focus on a subset of methods and compare them in depth. Finally, we discuss tractography applications to brain tumors and TBI and outline the prospects of novel tractography modalities as tools for exploring and understanding brain diseases.

It is noteworthy that there are several terminology conventions used in tractography to describe brain connections. Here and throughout, *tract* refers to macroscopic white matter pathways, such as the corticospinal tract and other white matter tracts. By contrast, *track* (or *streamline*) refers to the inferred trajectories of underlying tracts, as calculated

* Corresponding author at: Department of Neurological Surgery, UPMC Presbyterian, Suite B-400, 200 Lothrop Street, Pittsburgh, PA, 15213, USA.
E-mail address: frank.yeh@pitt.edu (F.-C. Yeh).

https://doi.org/10.1016/j.neuroimage.2021.118651.
Received 10 March 2021; Received in revised form 5 October 2021; Accepted 11 October 2021
Available online 18 October 2021.

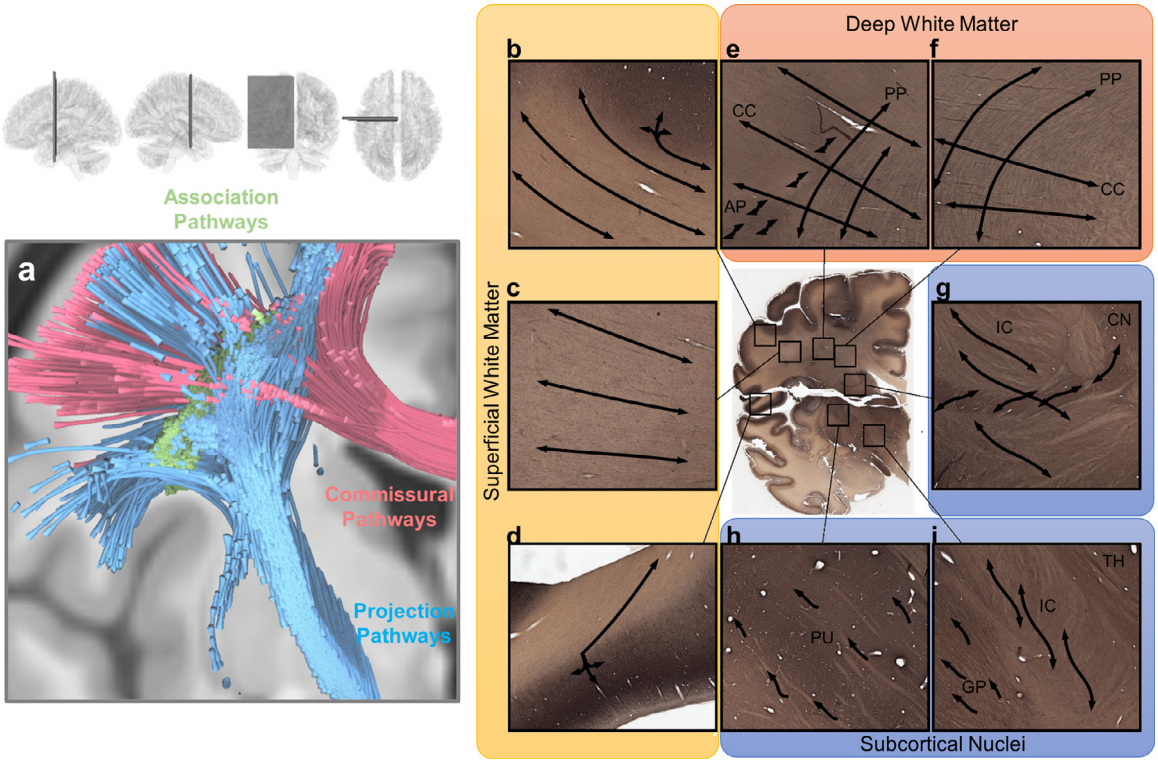

Fig. 1. Visualization of white matter pathways in the human brain and of challenges in mapping them across various white matter regions. (a) Brain pathways can be categorized into association pathways (green), projection pathways (blue), and commissural pathways (red). Mapping these pathways involves different challenges in different brain regions. (b), (c) and (d) show gyral blades in the superficial white matter on an immunohistochemistry section of a 34-year-old human brain. Connections with abrupt turning angles are often ignored in fiber tracking, leading to bias in tractography. (e) and (f) show deep white matter where corpus callosum (CC) bundles intersect projection pathways (PP) or association pathways (AP), demonstrating the challenge of mapping crossing tracts. (g), (h) and (i) show the white matter around subcortical nuclei. (g) enlarged view of the internal capsule (IC) and caudate nuclei (CN). The connections from caudate nuclei are small pathways, and mapping them requires higher angular and spatial resolution. (h) shows the putamen (PU), whereas (i) shows the boundary between the globus pallidus (GP), internal capsule (IC), and thalamus (TH). The fibers within the basal ganglia are often undetectable in dMRI due to the heavy T_2-weighting caused by iron complex deposition.

by a fiber-tracking algorithm; such tracks include *spurious tracks*, which are colloquially referred to as *false tracks*. *Fiber* refers to a tract population within a voxel, where each population is oriented in a distinctly different direction. The term is used in expressions such as *crossing fibers*, which describes two or more tracts at a voxel, or *fiber resolving methods*, which refer to methods that resolve local white matter tract orientations at each voxel.

2. Challenges in mapping brain pathways

Common tractography targets can be classified into the association, projection, and commissural pathways. As shown in Fig. 1a, the association pathways (green), such as the arcuate fasciculus and cingulum, constitute the superficial and deep white matter structures. The projection pathways (blue) are vertically projecting tracts connecting cortical regions to subcortical nuclei or brainstem regions. The commissural pathways (red), such as the corpus callosum, are connections between the left and right hemispheres. They often pass through the deep white matter and intersect with association and projection pathways. We further show histology images from a coronal section of the thalamus and basal ganglia in the BrainSpan reference atlas (https://www.brainspan.org/) (Miller et al., 2014) to illustrate the challenges in mapping white matter tracts. Fig. 1b-i are parvalbumin-labeled immunohistology, which present line strips in the white matter to reveal fiber bundles' gross orientations. The superficial white matter, deep white matter, and subcortical nuclei pose three distinct challenges to fiber tracking:

2.1. Gyral bias

The first challenge is the *gyral bias* of tractography at the superficial white matter (Reveley et al., 2015; Schilling et al., 2018a). As shown in Fig. 1b-d, superficial white matter comprises *gyral blades*, which are bulging structures with fanning fibers aggregated into bundles (Cottaar et al., 2020). In this region, most fiber tracking algorithms, including probabilistic and deterministic, tend to track the least turning trajectories to the gyral tip (e.g., the left three trajectories in Fig. 1b) and ignore those with an abrupt turning to the sulcal band (e.g., the turning trajectories in the right-upper corner in Fig. 1b). This least-turning preference avoids an abrupt turning that will produce considerable false turning in other white matter regions. However, in the superficial white matter, the resulting tractography only visualizes connections toward the gyral tip while ignoring many others along sulcal banks, leading to the false-negative mapping of the superficial pathways.

2.2. Crossing, turning, branching, and fanning structures

The second challenge of tractography occurs in the deep white matter (Fig. 1e and f), where tract bundles from different brain regions meet and intersect. The challenge here is to resolve the crossing, turning, branching, and fanning architectures formed by these pathways (Grisot et al., 2021). Many of them coexist within a white matter region, and thus resolving all of them could be a challenge. For example, fiber tracking methods may fail to capture the lateral fanning branches of the corpus callosum or projection pathways due to their relatively small sizes in this fiber crossing region (Reveley et al., 2015). The deep

white matter region in Fig. 1e and f, known as the *centrum semiovale* (CS), has three sets of pathways intersecting in a grid-like structure (Wedeen et al., 2012). The association pathways (as shown by label AP in the figure) such as the super longitudinal and arcuate fasciculi are often located laterally relative to projection pathways. More medially, there are vertically-oriented projection pathways (PP) such as the corticospinal and corticothalamic tracts. Those pathways have lateral branches forming branching and fanning architectures that also intersect the association pathways. The corpus callosum (CC) bridges the two hemispheres and crosses both the projection and association pathways. Fig. 1e shows the intersection of these pathways. The corpus callosum passes across the entire region, whereas projection pathways are oriented vertically; the association pathways (AP) have tracts oriented along the anterior-posterior (through-slice) axis. Much of the crossing geometry involves sharp crossing angles, and diffusion modeling methods may only resolve one fiber and miss others. Consequently, a tracking algorithm may only map a portion of the white matter connections and yield false-negative results in the deep white matter regions.

2.3. Subcortical nuclei

The third challenge of tractography involves white matter structures around subcortical nuclei (Fig. 1g-i), which are *hubs* of brain networks. Fig. 1g shows the caudate nuclei (CN) and internal capsule (IC). The large tracts in the internal capsule are intertwined with small connections between the caudate nuclei and the basal ganglia. Tracking these small tracts between large projection bundles around subcortical nuclei would require higher spatial resolution acquisitions. Fig. 1h and i further zoom in to the basal ganglia, including the putamen (PU) (Fig. 1h) and globus pallidus (GP) (Fig. 1i). The architecture of the basal ganglia features neuronal clusters enmeshed within white matter structures. Iron deposition in the basal ganglia introduces heavy T_2-weighting into dMRI. Consequently, these regions yield low diffusion-weighted signals due to T_2 shine-through, and fiber orientations cannot be resolved. Tracking projection pathways down into the brainstem (not shown here) also has challenges due to limited spatial resolution, phase distortion, and related signal loss around the air space of the skull base (Sclocco et al., 2018). Among the above-mentioned brain regions, the subcortical nuclei and brain stem pose the most significant challenges to fiber tracking due to their complex fiber architecture and low dMRI signal quality.

3. Tractography methods—an overview

Tractography pipeline workflows can be divided into multiple steps, including preprocessing, fiber resolving, fiber tracking, and post-tracking processing (Fig. 2). The first step starts with preprocessing the diffusion-weighted images and proceeds with resolving fiber orientation(s) for each voxel. At the beginning of the pipeline, the images are often preprocessed to reduce eddy current distortion and phase distortion artifacts as well as other signal quality problems. Additional noise reduction or signal corrections can be conducted to improve the quality further. The acquisition optimization and preprocessing strategies are discussed in Section 4. After preprocessing, diffusion-weighted images and their associated *b-table* can be modeled using various fiber resolving methods to reconstruct one or multiple fiber orientations at each imaging voxel. There are various methods to resolve fibers, and they are discussed in Section 5. The results of this step empower fiber tracking algorithms to produce track trajectories that can be visualized using tractograms (see Section 6). Trajectories obtained via fiber tracking can be post-processed to generate clusters/bundles, discard unsatisfactory results, or classify clusters and bundles neuroanatomically. Fig. 2b shows a popularity survey of publicly available tractography tools or pipelines based on Google Scholar search results. The differences between these tools can be classified based on their fiber resolving and fiber tracking approaches, as listed in Fig. 2a.

4. Diffusion MRI acquisitions

The dMRI data are collected using diffusion-sensitization sequences (Stejskal and Tanner, 1965; Wu and Miller, 2017), such that the acquired signals are sensitive to the microscopic diffusion movements of water. The diffusion sensitization is achieved by adding one or more *diffusion sensitization gradients*, or simply *diffusion gradients*, to the pulse sequence. The diffusion gradients are added to the spin dephasing and rephasing stages of a spin-echo or a stimulated-echo sequence. Thus any spin diffusion parallel to the gradient directions will decrease MR signals by interfering with the dephasing and rephasing process. The orientation of the gradients is called *b-vector*, whereas the strength of ensemble diffusion sensitization is quantified by *b-value*, a collective product of diffusion time, diffusion gradient duration, and diffusion gradient magnitude. The MR signals without diffusion sensitization are thus called the b0 signals, whereas the signals with diffusion sensitization will have attenuation due to diffusion. Faster diffusion or higher diffusion sensitization leads to more signal attenuation, whereas slower diffusion or lower diffusion sensitization retains more signal intensity. The signal attenuation at different directions provides the critical information to probe into the microscopic characteristics of the scanned tissue. In clinical applications, the optimization of a diffusion sequence considers scanning time, b-value, diffusion sampling scheme, distortions, and artifacts. We discuss each of them in the following:

4.1. Scanning time

The scanning time is a significant consideration in clinical applications. Diffusion MRI used to take a much longer scanning time than other MR modalities due to the need to acquire data at multiple diffusion directions. The development of simultaneous multi-slice acquisitions (Breuer et al., 2005; Setsompop et al., 2012a; Setsompop et al., 2012b) have allowed for reducing the scanning time by 2 to 4 folds. The shorter scanning time allows for more diffusion sampling directions, better slices coverage, or spatial resolution. For scanning patient populations, simultaneous multi-slice acquisition is a critical technique to reduce the scanning time. Ideally, a clinical study would limit dMRI acquisition to around 10 minutes. A shorter acquisition also reduces motion and signal quality issues associated with long scanning time.

Although simultaneous multi-slice acquisitions are practical solutions to reduce the scanning time, an under-recognized issue is the increased T_1 shine-through due to the reduced repetition time (TR). As more methods are introduced to achieve a higher acceleration factor, the reduced repetition time may eventually introduce substantial T_1 shine-through that decreases the diffusion signal. Pathological conditions that induce large T_1-weighting will further cause unexpected bias in diffusion-weighted images.

Besides using simultaneous multi-slice acquisitions, another strategy to reduce scanning time is to reduce the number of slices at the cerebellum. For the imaging brainstem or thalamus, the dMRI data can be acquired using fewer sagittal slices that cover only the targeted brain regions. Nonetheless, reducing the slices number also reduces TR and possibly introduces T_1 shine-through issue mentioned above.

4.2. B-value

The second consideration in diffusion MRI acquisition is the b-value, which determines the diffusion contrast at different diffusion directions. The diffusion contrast enables a modeling method to resolve principle diffusion directions as fiber orientations. A higher diffusion sensitization will lead to higher diffusion contrast but will also have more signal decrease. A lower diffusion sensitization will retain the signal intensity but may not generate enough diffusion contrast to model the diffusion patterns. Recent studies have suggested the benefit of a high b-value in sensing restricted diffusion and resolving complex axonal architectures

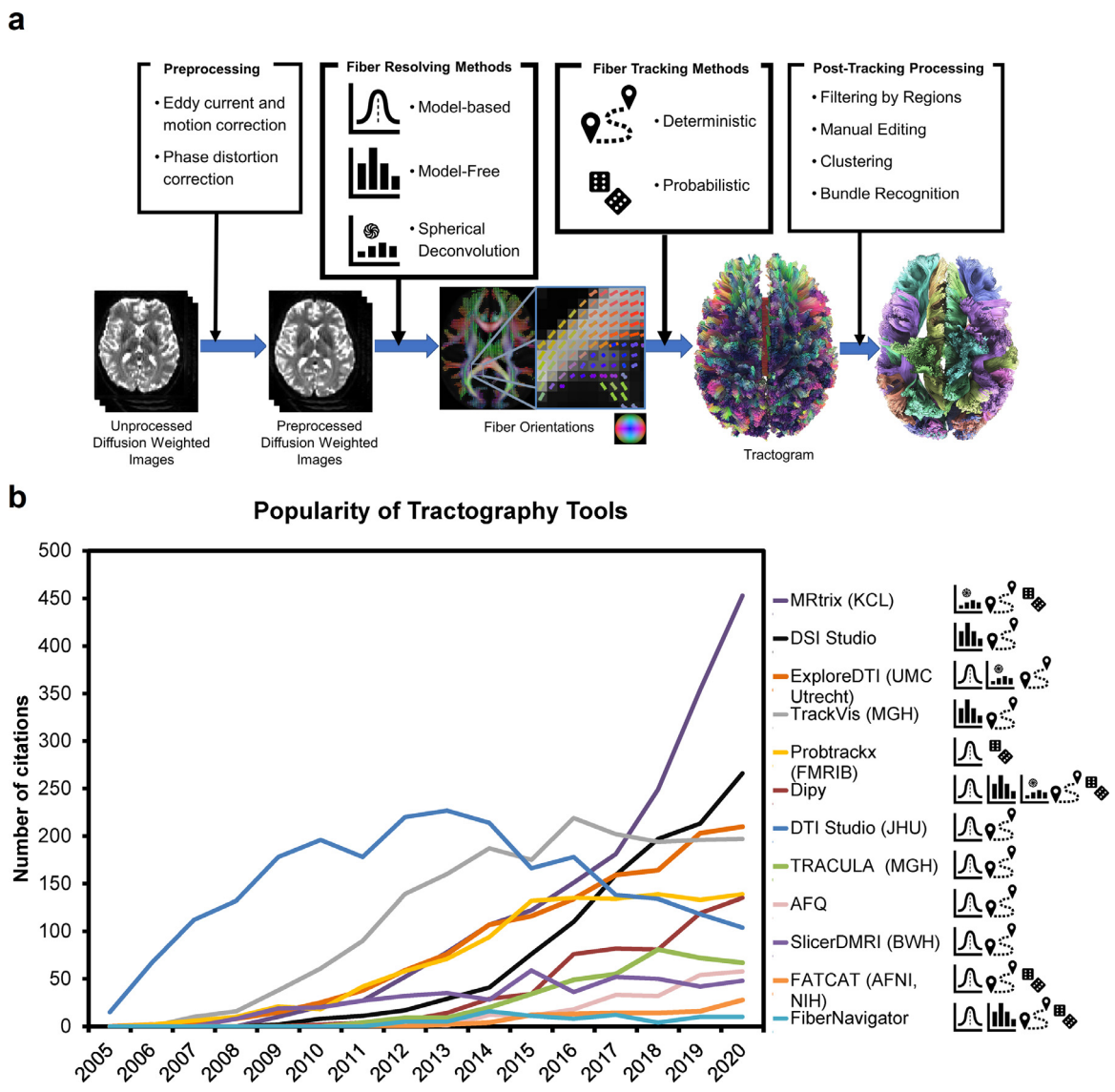

Fig. 2. Overview of tractography pipelines. (a) shows the snapshot of a typical tractography pipeline. The raw diffusion-weighted images are often preprocessed to remove eddy current and phase distortion artifacts or address other signal-related issues. The preprocessed images are then used to resolve fiber orientations and their associated diffusion metrics at each voxel. This information is then used by a fiber tracking method to produce tractograms for further post-processing. The tractogram can be color-coded by directional color (left-right: red anterior-posterior: green superior-inferior: blue) or by arbitrary colors after post-processing to visualize different bundles. (b) The popularity of publicly available tractography tools quantified by the number of Google Scholar search results from 2005 to 2020. The icons on the right label each tool's methodological category (see (a) for the legend).

(Fan et al., 2014; Genc et al., 2020; Yeh et al., 2019). For clinical applications, a higher b-value can achieve a better sensitivity to early neuronal change. The optimal value depends on spatial resolution and any parameters that can affect the signal intensity. A way to determine whether the b-value is too high is to inspect the resulting diffusion-weighted image and examine whether the cortex contour is still visible. Currently, most studies limit the highest b-values below 5000 s/mm^2, as long as there are enough signals in the gray matter after diffusion sensitization.

4.3. Sampling scheme

A diffusion sampling scheme defines the combination of b-values and b-vectors used in the dMRI acquisition. Commonly used schemes include single-shell scheme, multi-shell scheme, and grid scheme. The naming is based on the spatial distribution of the diffusion gradients in the *q-space*, a gradient encoding space similar to k-space. The readout gradients encode the k-space signals, whereas the diffusion gradients encode the q-space signals. Applying Fourier transform to the k-space signals will derive the spatial distribution of spins, whereas applying the inverted Fourier transform to the q-space signals will derive the displacement distribution of spin in the diffusion process. Each diffusion sampling scheme has its strength and weakness:

4.2.1. Single-shell scheme

The single-shell scheme acquires only one non-zero b-value at multiple diffusion directions, and thus the distribution of the diffusion gradients appears like a shell in the q-space. Examples of single-shell acquisitions include DTI acquisition and high angular resolution diffusion imaging (HARDI)(Tuch et al., 2002). Due to the single b-value used in the acquisition, the single-shell scheme is known for its limitation in differentiating different restricted diffusions, such as the hindered and restricted diffusion (Assaf and Basser, 2005; Assaf et al., 2004). Shell-like schemes densely sample *orientational* information to resolve fiber orientations, but it does not have enough *radial* information to resolve

Table 1
Diffusion schemes and their applicable methods.

	model-based methods											
	tensor-based				beyond-tensor		model-free methods				spherical deconvolution	
	DTI	BSM	FEW-DTI	multi-tensor	DKI	NODDI	DSI	QBI	GQI	MAP-MRI	CSD	MSMT-CSD
single-shell	x	x	x	x				x	x	x	x	
multi-shell	x	x	x	x	x	x		(x)*	x	x		x
grid	x	x	x	x	x	x	x		x	x		

x: applicable without resampling
*: only with constant solid angle QBI
DTI: diffusion tensor imaging, BSM: ball-and-sticks model, FEW-DTI: free water elimination DTI, DKI: diffusion kurtosis imaging, NODDI: neurite orientation dispersion and density imaging, CSD: constrained spherical deconvolution, MSMT-CSD: multi-shell multi-tissue CSD, DSI: diffusion spectrum imaging, QBI: q-ball imaging, GQI: generalized q-sampling imaging, MAP-MRI: Mean apparent propagator (MAP) MRI

different restricted diffusions. Methods based on single-shell acquisition are thus more susceptible to the partial volume of free diffusion caused by tissue edema, leading to possible false findings in tractography.

4.2.2. Multi-shell scheme

Multiple-shell acquisition addresses this limitation by acquiring 3~5 b-values with each b-value sampled at ~100 directions. The scheme thus presents multiple shells in the q-space and allows for differentiating different restricted diffusion. Examples include the hybrid diffusion imaging (Wu and Alexander, 2007) and the three-shell scheme used in the Human Connectome Project (Van Essen et al., 2012). Typically, low-b-value shells can be acquired by fewer sampling directions due to their lower diffusion contrast. The multi-shell acquisition will allow beyond-DTI methods to differentiate restricted diffusion and correlate with tissue characteristics.

4.2.3. Grid scheme

Still, some schemes do not use shell-like diffusion sampling. The grid scheme uses Cartesian sampling and is also known as *q-space* imaging (Callaghan, 1991). Similar to k-space imaging that usually samples MR signals at Cartesian locations, q-space imaging also samples at Cartesian points, and the scheme forms a grid sampling pattern. The resulting b-table often has 20~30 b-values with a total of 200~500 directions. The lowest non-zero b-value usually has only three directions, and the number of directions increases with the b-values. The multiple b-value setting of the grid scheme allows for fully characterizing a spectrum of restricted diffusion (Wedeen et al., 2005).

4.2.4. Choice of schemes

The choice between single-shell, multi-shell, and grid schemes largely depends on their applicable modeling methods. It is noteworthy that a scheme can work with many different modeling methods and vise versa. As listed in Table 1, the single-shell scheme, including the DTI dataset, can also be analyzed by other advanced methods, and similarly, an advanced scheme such as multi-shell or grid schemes can also be used by DTI. Single-shell schemes focus on *orientational* information because of their numerous sampling directions, but the single b-value setting does not have *radial* information to differentiate a spectrum of restricted diffusions. In comparison, a grid scheme focuses more on radial information by acquiring more than 10 b-values. The acquired data can be used to differentiate a spectrum of restricted diffusion. For clinical applications, the prevalence of pathological conditions would need multi-shell or grid schemes to characterize diffusion and correlate it with different pathological conditions.

4.4. Distortions and artifacts

Distortions and artifacts are common in dMRI acquisition because of the increased echo time to include the diffusion gradients. Commonly seen distortions and artifacts in dMRI include eddy current distortion and susceptibility-induced distortion. Other signal issues include gradient nonlinearity and signal drift. Although correcting all of them is the goal, some corrections may require additional scanning time, while some may not be readily correctable. For cost-effectiveness, a compromise for clinical application would prioritize those with more significant effects.

4.4.1. Eddy current distortion

The most significant distortion in dMRI is caused by the eddy currents. The eddy current will interfere with the signal readout and generate a different shear distortion at each diffusion-weighted image. Its effect is global and readily visible on the anisotropy map or final tractography results, characterized by artificially high anisotropy and spurious fibers on the brain surface. Due to its wide-spreading effects across the brain regions, correcting eddy current distortion is always necessary and can be done by preprocessing or sequence design. FSL's *eddy* (FMRIB, Oxford)(Andersson and Sotiropoulos, 2016) is the most commonly used preprocessing approach for eddy current correction. It uses a Gaussian process to estimate the expected image (Andersson and Sotiropoulos, 2015) and calculate its transformation to the actual collected image. The correction is then achieved by inverting the distortion, and the process simultaneously handles additional rotation and translocation due to head motion.

Nonetheless, the Gaussian process in FSL's *eddy* needs sufficient data redundancy and only works on shell schemes. At a b-value of 1500 s/mm^2, at least 10~15 diffusion sampling directions are required to provide enough data redundancy (Andersson and Sotiropoulos, 2015), and higher b-values would need more sampling directions and scanning time to enable the correction. For data acquired by non-shell schemes or insufficient sampling directions, the correction can be achieved using bipolar diffusion gradients (Finsterbusch, 2009; Reese et al., 2003; Yang and McNab, 2019). These sequence-based eddy corrections may provide an alternative solution to cancel the eddy current and eliminate distortion. Some diffusion gradient designs (Aliotta et al., 2018) further achieved a shorter echo time to improve the signal performance.

4.4.2. Susceptibility-induced distortions and artifacts

Another prominent distortion in dMRI is the distortion and signal dropout caused by susceptibility-induced magnetic field gradients at the tissue junction. For echo-planar imaging, the susceptibility gradients parallel to the slice plane will cause geometric distortion, whereas the gradients perpendicular to the slice will cause signal dropout. The effects are most prominent at the prefrontal, orbitofrontal, and inferior temporal regions if the phase encoding direction is oriented at the anterior-posterior direction. Since the effect is more focal than global, some studies may ignore it as a compromise if their region of interest has no detectable distortion or signal dropout.

Correction can be achieved by FSL's *topup* (FMRIB, Oxford)(Andersson et al., 2003), a preprocessing approach that estimates

the distortion field to undo the effect through regularized optimization. The minimal requirement is an additional field map or an additional b0 acquired at the opposite phase encoding direction. However, the induced distortion may not be fully restored at regions with a large susceptibility gradient, and the signal dropout can be uncorrectable. In such a condition, an effective strategy is to combine multi-shot EPI sequences (Butts et al., 1994; Holdsworth et al., 2008) to minimize susceptibility effects, while the residual distortion can be subsequently corrected by *topup*.

4.4.3. Other signal issues

Besides artifact and distortions mentioned above, other quality issues include gradient nonlinearity (Malyarenko et al., 2014; Tan et al., 2013), Gibbs ringing artifact (Perrone et al., 2015; Veraart et al., 2016), and signal drift (Hansen et al., 2019; Vos et al., 2017). Gibbs ringing is often deemed insignificant in dMRI because it is only visible at the sharp edge in high-resolution b0 images. The effect caused by gradient nonlinearity is often close to the noise level in lower SNR acquisitions (Mesri et al., 2020), and not all modeling methods are significantly affected (Guo et al., 2021). Similarly, signal drift only affects up to 5% of the signals in a 15-min scan (Hansen et al., 2019; Vos et al., 2017). For scans that use a shorter scanning time, the effect is close to the noise level. Thus, these signal issues are not routinely corrected due to relatively insignificant effects on the diffusion metrics and tractography results.

4.5. Quality control

Quality control is a critical component in dMRI analysis because the diffusion contrast is generated by diffusion-induced signal attenuation. Signal loss due to quality issues can mimic diffusion signal attenuation and consequently lead to spurious tractography results. Despite correction approaches mentioned above, some data may be too corrupted to be correctable due to various acquisition issues, and not all scan data are suitable for processing. Thus, quality control for dMRI should include a screening step to identify and exclude uncorrectable data.

Several automated tools are available for quality control purposes (Bastiani et al., 2019; Cai et al., 2021; Cieslak et al., 2021). These automated tools can generate a report for quality assurance or calculate quality metrics. For example, dMRI-based quality metrics (Cieslak et al., 2021; Yeh et al., 2019) are sensitive to subject motion, eddy current distortion, or volume-wise signal dropout. A substantially low value in these metrics indicates an acquisition issue that requires further inspection to determine whether the issue is correctable. After passing the screening, the data can be preprocessed to eliminate distortions and artifacts for further tractography analysis. In clinical applications, reports from automated quality control tools can be integrated as a quality assurance procedure to ensure the reliability of the results for diagnostic, prognostic, or interventional purposes.

5. Fiber resolving methods

After preprocessing, the dMRI data will be modeled by fiber resolving methods to estimate the fiber orientations at each imaging voxel (Fig. 2a). Methods to resolve fiber orientations can be categorized into model-based and model-free approaches. In the following subsections, we summarize fiber resolving methods and discuss their strengths and weaknesses.

5.1. Model-based methods

Model-based methods fit data samples based on pre-defined models or distribution functions, including the standard tensor model (Basser et al., 1994), two-tensor model (Qazi et al., 2009), free water elimination tensor (Pasternak et al., 2009), ball-and-sticks model (Behrens et al., 2003b), kurtosis model (Fieremans et al., 2011), or neurite orientation dispersion and density imaging (NODDI) model (Zhang et al., 2012). Model parameters provide fiber orientations for fiber tracking. One advantage of model-based approaches is that they often require fewer diffusion sampling directions than model-free methods. However, a common disadvantage is that the model assumptions can be violated due to the intricate diffusion patterns of biological tissues, particularly in the presence of gross pathology.

5.2. Model-free methods

Model-free methods seek to estimate orientation distribution functions (ODFs), which can be viewed as *histograms* quantifying the empirical distributions of diffusion at different orientations. ODF peaks can be used as fiber orientations for eventual tracking, and metrics can be calculated from ODFs to correlate with tissue characteristics. Model-free methods include diffusion spectrum imaging (DSI) (Wedeen et al., 2005), *q*-ball imaging (Aganj et al., 2010; Descoteaux et al., 2007; Tuch, 2004), generalized *q*-sampling imaging (GQI) (Yeh et al., 2010), and mean apparent propagator MRI (Ozarslan et al., 2013). These methods are also known as *q*-space imaging methods because they often rely upon the Fourier transform relation between diffusion distributions and *q*-space signals (Callaghan, 1991). Model-free methods often need more diffusion sampling directions and longer scanning time, but the strength is that they do not assume a specific diffusion model. This feature makes model-free methods ideal choices for clinical applications, where a disease or pathological condition may exhibit complex diffusion patterns caused by demyelination, hemorrhage, edema or infiltration of immune or tumor cells.

5.3. Spherical deconvolution

Spherical deconvolution (Tournier et al., 2004) and its derivatives (Dell'acqua et al., 2009; Jeurissen et al., 2014; Rokem et al., 2015; Tournier et al., 2007) leverage the strengths of both model-free and model-based methods. Similar to model-free methods, spherical deconvolution methods also calculate an ODF called the fiber orientation distribution (FOD). On the other hand, similar to model-based methods, spherical deconvolution methods use diffusion signals from selected fiber portions (i.e., the mid-sagittal part of the corpus callosum) as a diffusion model to design deconvolution kernels. These kernels are called *response functions* and are used as a unified diffusion model to resolve fiber orientations. The resulting FODs are often sharper and achieve relatively higher power to resolve crossing fibers. The multi-shell version of spherical deconvolution further provides tissue characterizations (Jeurissen et al., 2014).

5.4. Comparison

Fig. 3 displays fiber orientations calculated from diffusion tensors, diffusion ODFs, and FODs based on the same data from the first subject in the Penthera (Paquette et al., 2019) and traveling subjects dataset (Fig. 3a and b, respectively) (Tong et al., 2020). Fig. 3 data were generated using a cloud computation service provided by brainlife.io (Avesani et al., 2019) through its web applications of DSI Studio (http://ds-studio.labsolver.org) and MRtrix3 (Tournier et al., 2019). The diffusion ODF was calculated using GQI (Yeh et al., 2010), whereas the FOD was calculated using multi-shell, multi-tissue constrained spherical deconvolution (Jeurissen et al., 2014). The threshold for filtering fiber orientations was determined by a value that achieved the best consistency between the three approaches to facilitate comparison. The coronal slices in Fig. 3 are selected to include the thalamus and basal ganglia, thereby facilitating cross-reference with Fig. 1.

As shown in Fig. 3, the tensor model can only resolve one fiber orientation for each voxel in the centrum semiovale (CS), and thus DTI tractography cannot track the transverse branches of the corpus callosum (CC), as delineated by the dashed line. The fiber orientations re-

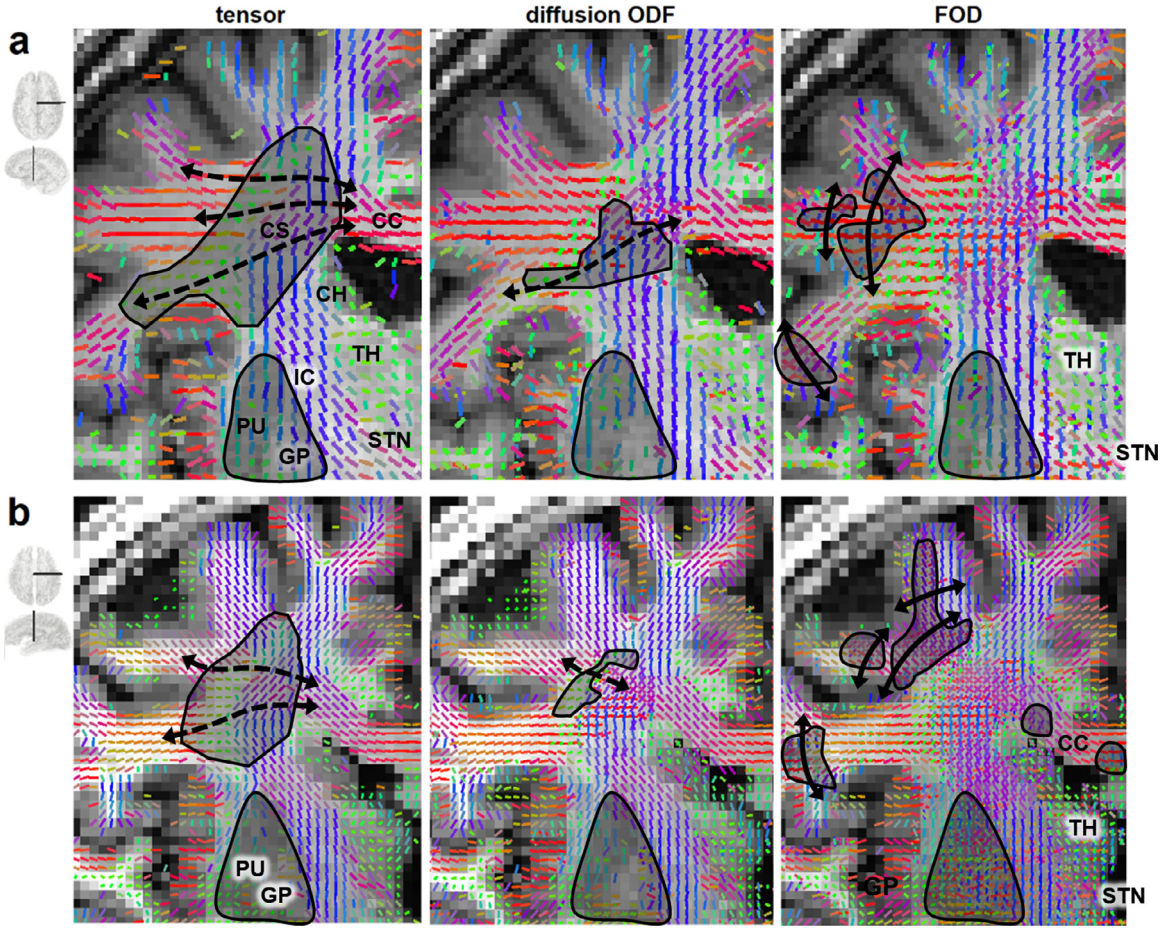

Fig. 3. Commonly encountered ambiguities in fiber orientations as resolved by the standard tensor model, diffusion orientation distribution functions (ODFs), and fiber orientation distributions (FODs). The illustrations are based on publicly available data from (a) the Penthera 3 T dataset (Paquette et al., 2019) and (b) the traveling subjects dataset (Tong et al., 2020). Data were processed using MRTrix3 and DSI Studio on a cloud computing platform (brainlife.io). The resolved fibers are shown by sticks colored by directional color (left-right: red, anterior-posterior: green, superior-inferior: blue). The tensor model (first column) only resolves one fiber orientation per voxel and cannot map the lateral branch of the corpus callosum (CC) (dashed line). The diffusion ODF model can resolve part of the crossing fibers but may still miss some lateral branches (dashed line) of the CC. FODs provide the highest resolving power for identifying crossing fibers but may occasionally produce arc-shaped spurious tracks perpendicular across the gyrus. The FOD results within the subthalamic nuclei (STN) and the thalamus may cause difficulties for tracking subcortical targets. For all three methods, the fiber orientations resolved for the putamen (PU) and globus pallidus (GP) are unreliable due to heavy T_2-weighting caused by iron complex deposition. .

solved in the putamen (PU) and globus pallidus (GP) are unreliable due to weak dMRI signals. Nonetheless, the showcased limitation in resolving crossing fibers does not imply that DTI tractography is unusable in such cases. Specifically, DTI tractography has been used to track association pathways such as the arcuate fasciculus (Glasser and Rilling, 2008; Rilling et al., 2008; Saur et al., 2008) and the superior longitudinal fasciculus (Karlsgodt et al., 2008; Makris et al., 2005; Martino et al., 2013). Moreover, in the subcortical structures, DTI tractography has shown clinical benefit in mapping pathways near the thalamus (TH) and subthalamic nucleus (STN) for deep brain stimulation (Coenen et al., 2011; Vanegas-Arroyave et al., 2016). The accuracy of DTI tractography thus depends on white matter location, and researchers should be aware of DTI limitations in mapping crossing fibers.

Diffusion ODF can resolve fibers crossing at angles between 45 and 90 ° (Cho et al., 2008), but fibers crossing at smaller angles, such as those annotated by dashed lines in Fig. 3, cannot be resolved. As a result, tractography using diffusion ODF may still miss part of the callosal branches. Furthermore, diffusion ODF cannot resolve fibers at the putamen (PU) and globus pallidus (GP) due to iron deposition that causes low diffusion MRI signals. The primary strength of diffusion ODF tractography is its applications under various pathological conditions that dramatically alter the diffusion pattern (Abhinav et al., 2015; Becker et al., 2020; Celtikci et al., 2018; Zhang et al., 2013). Overall, tractography based on diffusion ODF offers improvements over DTI by providing better mapping of crossing patterns (Gangolli et al., 2017). However, the former method still requires cautious interpretation due to its potential failure to capture specific crossing configurations (Neher et al., 2015).

FOD tractography has a better resolving power than DTI and diffusion ODF methods (Tournier et al., 2008; Wilkins et al., 2015a), making it ideal for delineating fibers crossing at a sharp angle (Neher et al., 2015). However, FOD approaches may occasionally yield false identifications of fibers perpendicular to gyri. These false fibers may manifest themselves as arc-shaped false tracks in gyral blades, as shown by the black lines in Fig. 3a and b, whereas histology (Fig. 1b and c) show no fibers spanning across the gyrus. These false fiber tracings are often found at larger crossing angles between 50 and 90 ° (Parker et al., 2013) and may be caused by the mismatch of response functions since tract bundles in different brain regions may have distinct diffusion patterns

(Schilling et al., 2019a). FOD tractography is usually more sensitive to crossing fibers, but attention should still be devoted to potential false findings (Knösche et al., 2015).

With many different fiber tracing methods available, researchers should take into careful consideration each method's pros and cons and their differential suitability for different brain regions and fiber tracing goals. This advice is supported by a recent histology study suggesting that fiber resolving methods can have different performances in different brain regions (Schilling et al., 2018b). For example, FOD tractography is often ideal for capturing sharp crossings, such as in the lateral branches of the projection pathways or corpus callosum (Jeurissen et al., 2011; Wilkins et al., 2015b). On the other hand, model-free methods can facilitate the study of various pathological conditions (e.g., TBI, encephalopathies, tumors), where fibers undergo demyelination or edema that induce deviations from normative diffusion models. In brain regions with no crossing fibers, DTI can still produce reliable tractography results (Kristo et al., 2013; Kristo et al., 2012). In mapping cardiac muscle fibers, DTI is still the method of choice for cardiac tractography (Sosnovik et al., 2009) due to its less stringent imaging requirements and to its lower risk of modeling crossing fibers inadequately. The fiber orientations resolved by any of these methods can be coupled with any fiber tracking method to generate tractography, as detailed in the next section.

6. Fiber tracking methods

Fiber tracking was initially addressed as a numerical estimation problem since its introduction 20 years ago (Basser et al., 2000; Mori et al., 1999). From a numerical perspective, the problem can be viewed as solving an *ordinary differential equation* (ODE), and the targeted track trajectory is the unknown function to be estimated. This numerical problem is often called the *first-order ODE problem* or *first-order initial value problem*. Fig. 4a uses a one-dimension function to visualize this numerical estimation process. The goal of the first-order ODE problem is to numerically estimate an unknown function (grayed dashed line) using both its first derivatives (black arrows) and an initial value of the function (black circle). In fiber tracking, the first derivatives of the function are the fiber orientations resolved by fiber resolving methods described previously, whereas the initial value is the *seeding point* used by fiber tracking algorithms to begin the fiber tracking process.

6.1. Euler method

One of the most popular numerical approaches to solving first-order ODEs is the Euler methoddue to its relative simplicity and adequate numerical stability. In fiber tracking, this method is used as an iterative approach to calculate fiber trajectories by iterating between a *direction estimation* step and a *propagation* step (Basser et al., 2000). The approach starts at a pre-defined starting location, $f(t_0)$, (a.k.a. the seed). The local fiber direction at this current location, $f/prime(t_0)$, is provided by the fiber resolving methods (e.g., the tensor model, diffusion ODF, or FOD mentioned in Section 5) and is used to define the propagation direction. The tracking process iteratively propagates the trajectory of the track in two opposing directions (Fig. 4a). At each iteration i, the spatial trajectory is extended by calculating $f(t_{i+1}) = f(t_i) + f/prime(t_i)\Delta s$, where Δs is a pre-defined distance called the *step size*. The above process is repeated until any of the termination criteria are met. Commonly-used termination criteria include (a) an anisotropy threshold (which terminates tracking if fractional anisotropy falls below a pre-defined value)(Yeh et al., 2013), (b) a brain mask (which terminates tracking if the end coordinate of a track falls outside the brain region) (Smith et al., 2012), and (c) an angular threshold (which terminates tracking if the fiber trajectory makes a sufficiently abrupt turn). Both deterministic and probabilistic fiber tracking often rely on this Euler estimation framework. The main typical distinction between approaches is whether the propagation direction is randomly selected from the distribution of directions (thus probabilistic) or whether it is determined before tracking begins (thus deterministic) (Descoteaux et al., 2009).

6.2. Errors in fiber tracking

The standard numerical analysis shows that the numerical errors of the Euler method are reduced linearly as step size decreases (i.e., using big-oh notation, O (Δs)); for higher-order methods such as the Runge-Kutta method, the reduction is quartic (i.e., O(Δs^4)). However, this error estimation does not consider other errors associated with unique scenarios of fiber tracking, as shown in Fig. 4b-d. The figures illustrate three scenarios whose mathematical setting deviates from that of a typical first-order ODE problem.

In Fig. 4b, the first scenario is the *angular deviation* in the local fiber orientation. The deviation can be due to artifacts, modeling limitations, partial volume effects, or interpolation errors. The diffusion MRI community has devoted efforts to address the angular deviation problem (Tournier et al., 2011); however, the best approaches may still have a typical angular deviation of 6 to 10 ° shown by histology (Schilling et al., 2016). Higher-order ODE solutions may not necessarily be more accurate since the trajectory error caused by angular deviation is often more substantial than those caused by the step size. The second scenario, illustrated in Fig. 4c, occurs at the boundaries of tract bundles. A bundle may have an end surface near the gray matter, but fiber tracking can have *premature terminations* or *overshoots* due to an error in the termination criteria. As shown in Fig. 4d, the third scenario involves the existence of multiple trajectories at the same location. Specifically, each imaging voxel can be associated with more than one fiber orientation, and fiber tracking could generate an incorrect routing that bridges two unrelated bundles and creates spurious tracks. All three scenarios can occur in combination with one another and greatly complicate the task of fiber tracking. For example, tracking may start with a minor deviation due to an error in fiber orientations and then wrongly connect a bundle to unrelated nearby bundles. Alternatively, tracking may fail to terminate, as appropriate, at the gray-white matter junction and may instead bridge another bundle across a sulcus. Thus, identifying false tractography results requires an adequate understanding of how fiber tracking may fail due to scenarios like those shown in Fig. 4b-d.

Fig. 4e lists examples of spurious bundles identified by experts when constructing a human brain tractography atlas (Yeh et al., 2018). The blue arrows in the figure point to incorrect routing that bridges two unrelated bundles, whereas the red arrows point to premature track terminations. While identifying premature terminations can be accomplished by referring to structural anatomy images (Smith et al., 2012), identifying incorrect routings often require prior anatomical insights and knowledge because incorrect routing bundles may still contain (mostly) realistic trajectories. Moreover, the trajectories of spurious tracks may match local fiber orientations and diffusion patterns (Maier-Hein et al., 2017), meaning that the dMRI dataset itself may not provide sufficient information to reject such false trajectories. In such cases, prior independent information (e.g., from a tractography atlas) may be needed to map white matter pathways correctly.

Throughout the past 20 years of tractography algorithm development, the neuroimaging community has acknowledged that fiber tracking methods typically yield a substantial number of spurious results that should not be ignored (Reveley et al., 2015; Thomas et al., 2014). Although numerous tractography competitions and challenges have been organized, most have not identified a clear winner favoring any particular fiber tracking method (Fillard et al., 2011; Maier-Hein et al., 2017; Pujol et al., 2015; Schilling et al., 2019b). This suggests that tractography's accuracy challenges are more substantially rooted within the intrinsic limitations of dMRI as a technique rather than within numerical methodology. Thus, there is a need for independent information and anatomical priors to achieve higher accuracy in fiber tracking. We discuss this trend further in Section 9.

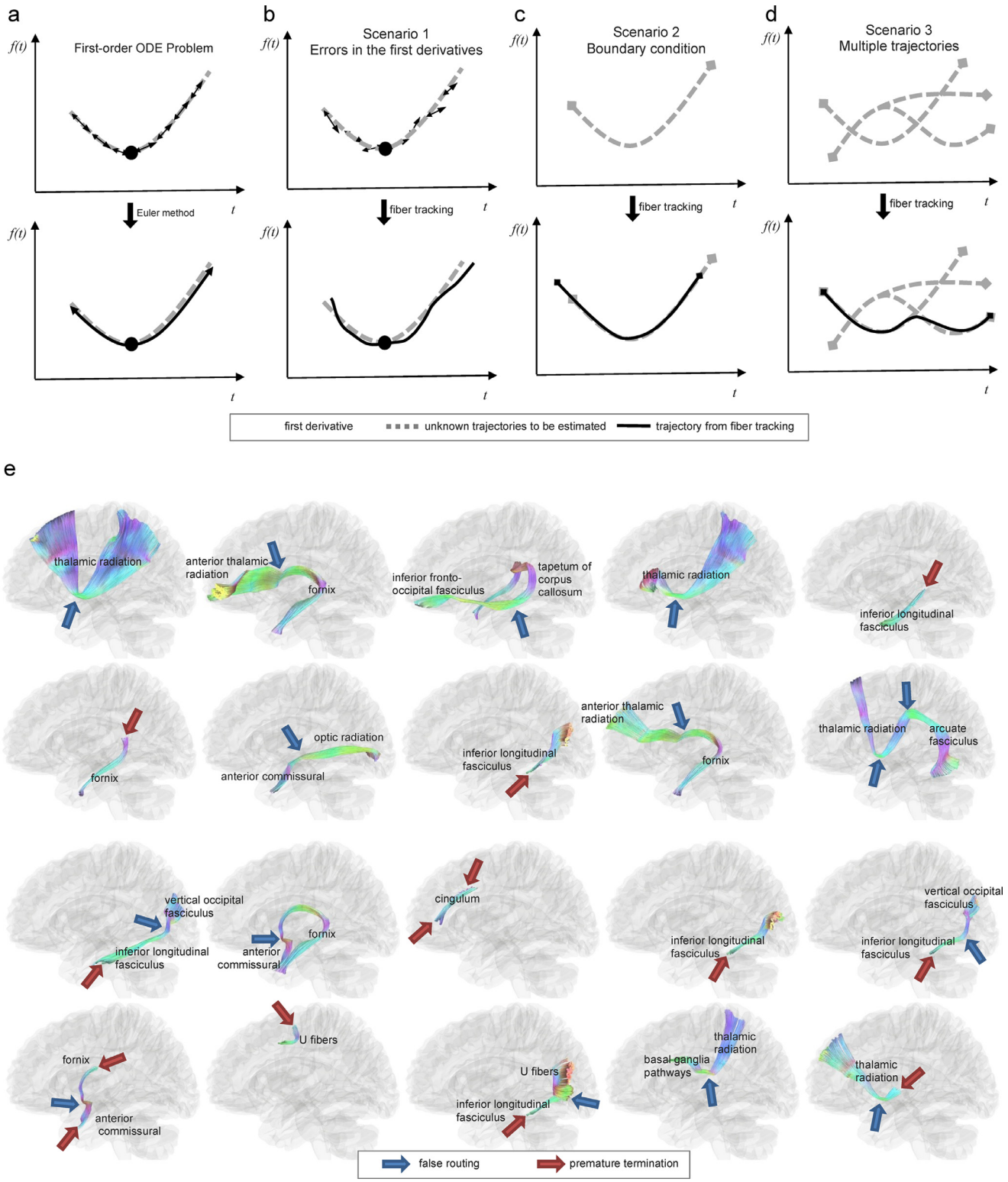

Fig. 4. Challenges in fiber tracking and examples of spurious tracks. (a) fiber tracking involves a numerical procedure to solve a first-order ordinary differential equation (ODE) whose parameters are specified by a starting location (i.e., the seeding point, black circle) and by the first derivative of a function (i.e., the resolved fiber orientation, arrows) at each voxel. The trajectory can then be calculated using the Euler method. However, the conventional ODE problem only considers numerical error due to finite step size and does not consider other error scenarios in fiber tracking. (b) The first scenario that raises challenges for standard fiber tracking involves errors in the estimation of first derivatives, which can cause substantial deviation of trajectories from their ground truth. (c) The second challenging scenario involves the boundary condition. Specifically, white matter tracts have termination locations, and fiber tracking may terminate at the wrong location, leading to a premature termination or an overshoot. (d) The third challenging scenario involves the coexistence of multiple trajectories at the same voxel location. Connecting unrelated trajectories may lead to incorrect streamline routing and spurious tracks. (e) example of spurious tracking results identified by neuroanatomists in an atlas construction study (Yeh et al., 2018). The tractogram is color-coded by directional color (left-right: red, anterior-posterior: green, superior-inferior: blue). The locations of incorrect routings and premature terminations are annotated by blue and red arrows, respectively. Incorrect routing is often due to a deviated tracking procedure that bridges two unrelated bundles and produces spurious trajectories. Identifying false results requires prior neuroanatomical knowledge—and even mapping nearby pathways–to rule out the possibility of incorrect routing.

7. Tractography in patients with brain tumors

Tractography has emerged as a standard tool in many institutions for preoperative assessment of white matter tracts perilesional to gliomas, primarily due to recent improvements in the image acquisition time and to the promising potential of its clinical applications (Henderson et al., 2020; Nimsky et al., 2005; Vanderweyen et al., 2020). To achieve optimal surgical outcomes, studies have demonstrated that maximal tumor resection is an independent prognostic factor for survival in high- and low-grade gliomas (Jakola et al., 2013; Lacroix et al., 2001; Li et al., 2016), whereas neurological deficits after resection of tumors are associated with a decrease in overall survival and quality of life (Rahman et al., 2017). For preoperative assessment, a safe maximal resection has been the surgical goal in brain tumor patients. To this end, tractography's primary role is to provide individualized reconstructions of tract trajectories and to reveal the relationship between the lesion and critical white matter tracts, thereby aiming to assist maximal tumor resection while avoiding new postsurgical deficits.

7.1. DTI tractography in brain tumors

Early in tractography development, DTI tractography was used to depict the pathological effects of brain tumor growth on white matter pathways, including infiltration, displacement, disruption, and destruction of tracts (Witwer et al., 2002). At least one study also showed good correspondence between positive subcortical stimulation sites and language tract mapping by DTI tractography (Leclercq et al., 2010a), although false-negative results require attention. Later studies have shown that tractography-based navigation associated with subcortical mapping contributes to maximal safe resection of cerebral gliomas involving the corticospinal tract (CST) (Wu et al., 2007; Zhu et al., 2012; Zolal et al., 2012). In low-grade gliomas, critical areas around the tumor, both cortical and subcortical, are among the most important factors limiting the extent of resection (Hervey-Jumper and Berger, 2019). Intra-tumoral DTI tractography in cases of low-grade gliomas has revealed that the presence of motor and language pathways within the tumor can predict eloquent areas and the extent of resection (Mato et al., 2021). In practice, preoperative tractography can be incorporated into surgical navigation devices to provide a three-dimensional visualization of white matter tracts of interest and their relationship to critical anatomical structures during surgical planning and resection (Coenen et al., 2001; Kuhnt et al., 2012; Nimsky et al., 2006) (Fig. 5). Functional MRI activation areas can be used as seed regions of interest for DTI tractography (Smits et al., 2007), resulting in better prediction of functional fascicles than anatomical-based tractography (Sanvito et al., 2020). Tractography data can be interactively visualized by the surgeon using dynamic seeding and region of interest to demonstrate the relationship of white matter tracts to the lesion and critical structures (Fekonja et al., 2019; Golby et al., 2011).

More recently, laser interstitial thermal therapy has become an increasingly used, minimally invasive, image-guided treatment option for patients with some brain tumors. In this procedure, a laser fiber is stereotactically inserted into the lesion to heat the tissue under MR thermometry and to ablate the lesion. Tractography can also be incorporated into pre- or intra-operative images to guide the safest approach trajectory and ablation of lesions (Fig. 6).

Overall, DTI tractography has helped neurosurgeons correctly identify patients with interrupted white matter tracts in whom a more aggressive extent of tumor resection can be pursued (Alexopoulos et al., 2019). The knowledge of the location and integrity of critical pathways is crucial to the neurosurgeon to preserve eloquent subcortical white matter and to avoid postoperative neurological deficits (Tuncer et al., 2021). Nonetheless, it is noteworthy that negative findings in DTI tractography are not sufficient to rule out the existence of functional tract pathways in the peritumoral region (Leclercq et al., 2010a).

In addition to trajectories obtained from tractography, the diffusion metrics associated with this technique can inform clinicians about the integrity of peritumoral white matter pathways. The combination of quantitative information along trajectories can provide clinically relevant information on the location and integrity of peritumoral tracts in a lesion vicinity. Clinically relevant findings include the destruction of tracts by aggressive lesions such as high-grade gliomas, infiltration by low-grade gliomas, and displacement by metastases or meningiomas, although any or all of these can co-occur (Young and Knopp, 2006). When integrated with track-based metrics, tractography can provide surgeons with qualitative and quantitative information regarding potentially affected tracts around an intracranial lesion. In DTI tractography, the tensor model provides fractional anisotropy (FA), which may reflect changes in tract integrity, and apparent diffusion coefficient (ADC), which may reflect changes in the perilesional area such as an increase in cellularity. These metrics have been used to evaluate the perilesional zone around gliomas, mainly to help distinguish infiltration from edema (Hoefnagels et al., 2014; Provenzale et al., 2004). However, it is noteworthy that FA and ADC can be affected by various factors (Alexander et al., 2001; Hui et al., 2010; Pasternak et al., 2009), and that changes can be nonspecific. Consequently, their clinical values in the diagnostic and prognostic evaluation are limited due to their relatively low specificity and sensitivity.

Tractography can also assist stereotactic radiosurgery (SRS) planning. SRS is a highly conformal treatment used to treat some brain tumors (and other lesions). SRS delivers a high dose of radiation in one, or up to five, treatment sessions. Reports in the literature have suggested that white matter tracts, particularly the optic radiation and arcuate fasciculus, are more vulnerable to radiation during SRS than previously thought (Maruyama et al., 2007; Maruyama et al., 2009). For treatment planning, DTI tractography images can be fused with stereotactic treatment images to analyze dosimetry for critical tracts (Maruyama et al., 2005). Integrating DTI tractography into SRS planning has been reported to help prevent morbidity related to radiosurgery in patients undergoing treatment for arteriovenous malformations (Koga et al., 2012). There is support for the view that delineation of functional structures and tracts in dosimetry planning is beneficial and could reduce the dose received by these healthy tissues, thus decreasing the risk of radiation-induced complications and increasing the quality of the delivered treatment (Pantelis et al., 2010). In a study with 23 patients with lesions adjacent to the CST where DTI-tractography was fused with stereotactic MRI, the CST was treated as an at-risk "organ," and the conformal dose was planned; clinical parameters between plans with and without tractography were then evaluated (Kawasaki et al., 2017). The maximum CST dose was significantly reduced by tractography planning, adding only a 3.5 min irradiation time prolongation. There was no significant difference in the dose covering 95% of the lesion volume (D95). The results suggested that the CST dose can be reduced while maintaining the D95 with clinically acceptable prolongation of the irradiation time (Kawasaki et al., 2017). Integration of tractography into SRS represents a promising tool for preventing radio-induced toxicity and complications (Maruyama et al., 2007).

7.2. Limitations of DTI tractography in brain tumors

DTI tractography and diffusivity-based measurements have several limitations despite their widespread clinical use. To recapitulate, the tensor model cannot describe multiple fiber orientations, and the estimation of axonal directions can be inaccurate in regions with crossing fibers (Alexander et al., 2001; Tuch et al., 2002). Moreover, a tumor can disrupt, displace, and infiltrate white matter while simultaneously causing peritumoral edema. Pure vasogenic edema is found around some meningiomas and metastatic lesions, whereas infiltrative gliomas can have vasogenic edema and neoplastic infiltration (Min et al., 2013). The diffusivity-based measurements can also be over-estimated or under-estimated due to cell infiltration or peritumoral edema (Wang et al., 2011). DTI metrics, such as FA, can be affected by crossing fiber con-

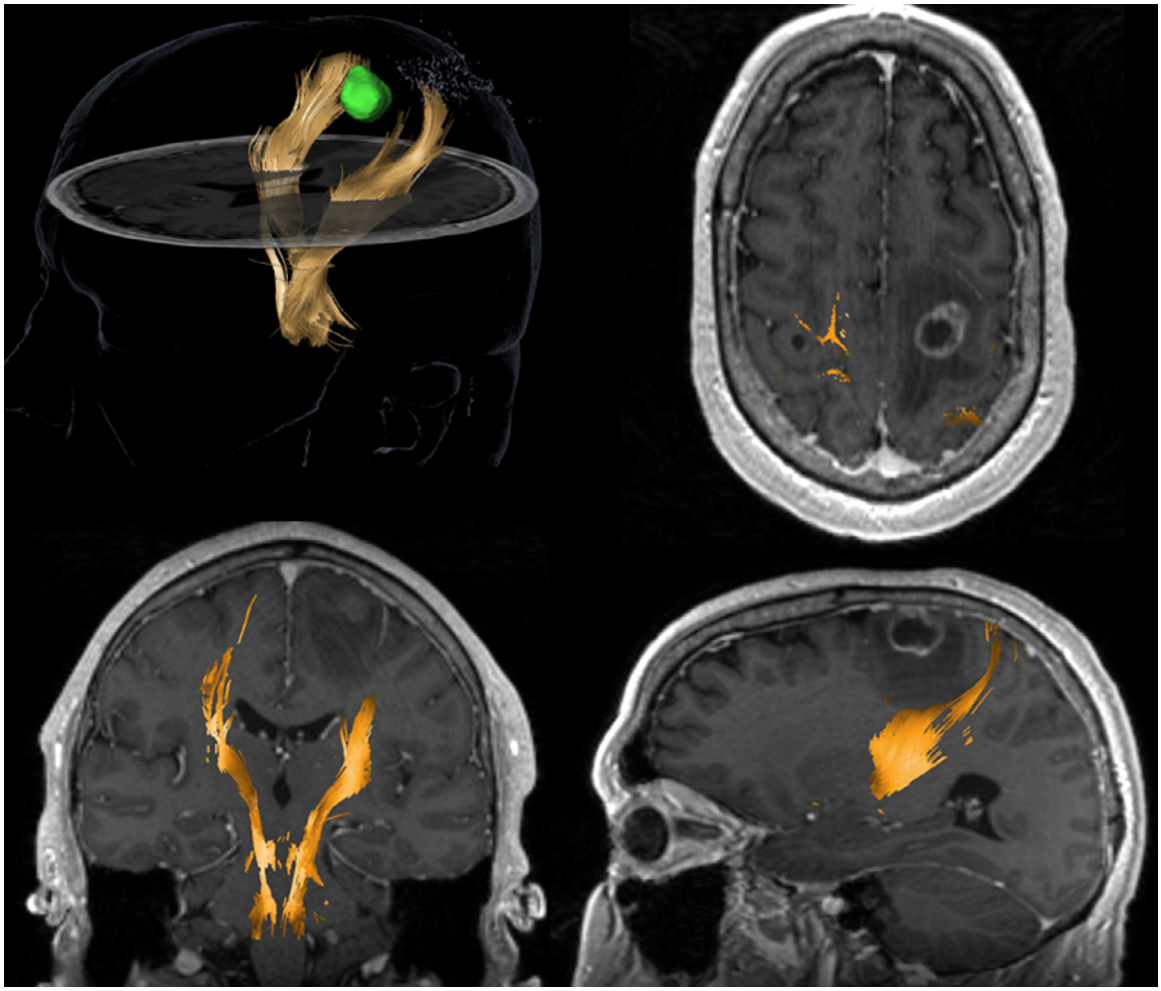

Fig. 5. DTI-based tractography from a surgical navigation system for a 58-year-old patient with non-small cell lung cancer which metastasized in the left frontoparietal region of the brain. The tracking used a multi-ROI (region of interest) approach with one cubic box positioned in the region of the posterior limb of the internal capsule, at the level of the interventricular foramina of Monro and another box placed at the anterior inferior pontine level, inserted caudally relative to the upper and middle cerebellar peduncle. The left corticospinal tract (yellow) is displaced posteriorly compared to the right (contralateral) branch. A region of hypointensity (low signal) around the lesion suggests vasogenic edema. It is crucial to notice that DTI tractography shows no tracks in the region of edema. This negative finding is likely due to the inability of DTI to track streamlines in edematous regions and does not unequivocally indicate tract disruption.

ditions or by partial volume effects in the edematous zone around the gliomas, which in turn can lead to premature termination of the fiber tracking and the risk for the incomplete reconstruction of a perilesional tract (Chen et al., 2015b)(Fig. 7). Change in the free water content of tissue lowers FA values, while the tracts might remain unaffected. Consequently, DTI-based tractography can fail to demonstrate tracts that are present—but not traced—due to several types of tissue abnormality around brain tumors, such as edema or tumor cell infiltration (Leclercq et al., 2010b) (Zhang et al., 2013). This drawback can cause DTI tractography reconstructions to become inaccurate and inconsistent in edematous regions around tumors, making it harder to differentiate destroyed white matter tracts from intact ones with edematous white matter, a critical task for neurosurgical planning (Kinoshita et al., 2005; Schonberg et al., 2006).

7.3. Advanced tractography in brain tumors

Several advanced tractography methods have been proposed to address the limitations of DTI tractography in the presurgical planning for brain tumor surgery. Their advantages include more reliable results in the presence of peritumoral edema and complete mapping of tract branches. Specifically, Zhang et al. (2013) compared DTI and GQI tractography using preoperative and postoperative scans on brain tumor patients. The results showed that advanced tractography could comprehensively display existing tracts in the edema, whereas DTI tractograms were incomplete. Chen et al. (2015a) retrospectively compared DTI tractography with two-tensor unscented Kalman filter tractography and found that advanced tractography can provide better sensitivity in mapping arcuate fasciculus tractography in the presence of peritumoral edema. More recently, Gong et al. (2018) performed a similar retrospectively comparison in patients harboring tumors near the CST and reached the same conclusion. Several studies comparing DTI tractography with advanced tractography have confirmed that the latter can map white matter tracts with higher accuracy and better safety margins for neurosurgical procedures. (Abhinav et al., 2015; Christiaens et al., 2015; Farquharson et al., 2013; Fernandez-Miranda et al., 2012). The metrics from advanced modeling may further offer additional information over conventional DTI metrics (Fekonja et al., 2020). Thus, replacing DTI tractography with advanced tractography has been recommended (Nimsky, 2014). The latter can be color-coded with other imaging modalities to evaluate white matter tracts around a brain lesion for diagnostic and prognostic assessment. The integrated tractogram can inform the extent of peritumoral edema or tumor cell infiltrations and help clinicians achieve a safe maximal resection (Fig. 8a and b).

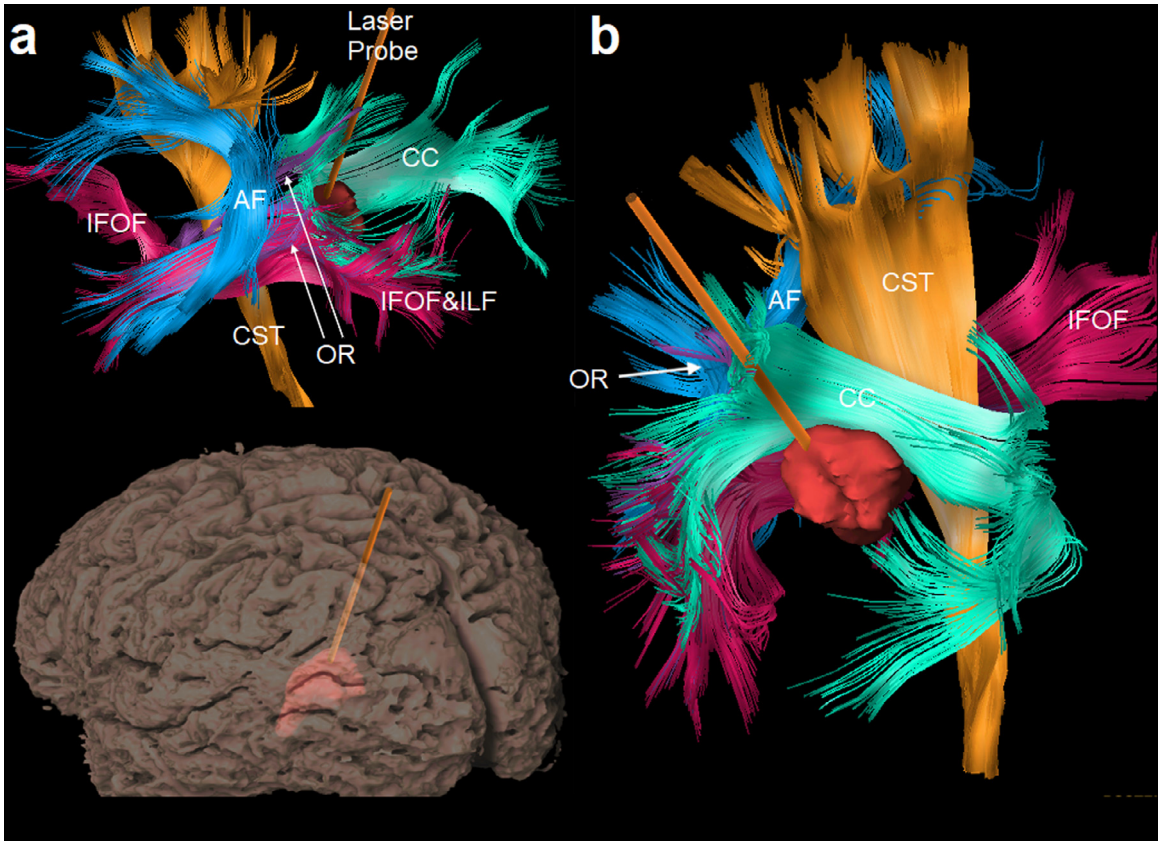

Fig. 6. Surgical planning for laser interstitial thermal therapy: an image-guided, minimally-invasive treatment that has been increasingly used to treat hard-to-reach primary or metastatic brain tumors. (a) Tractogram and the gyral surface viewed from the same left-posterior direction show a laser probe inserted into the tumor lesion to heat the tissue under MR thermometry and to ablate the lesion. Tractography of peritumoral pathways can be integrated with preoperative and intra-operative images to guide the safest ablation. Nearby tracts include the arcuate fasciculus (AF), corticospinal tract (CST), inferior frontal-occipital fasciculus (IFOF), inferior longitudinal fasciculus (ILF), optic radiation (OR), and corpus callosum (CC). (b) A view from the right-posterior-superior direction shows the relative location of the lesion to the surrounding critical tracts.

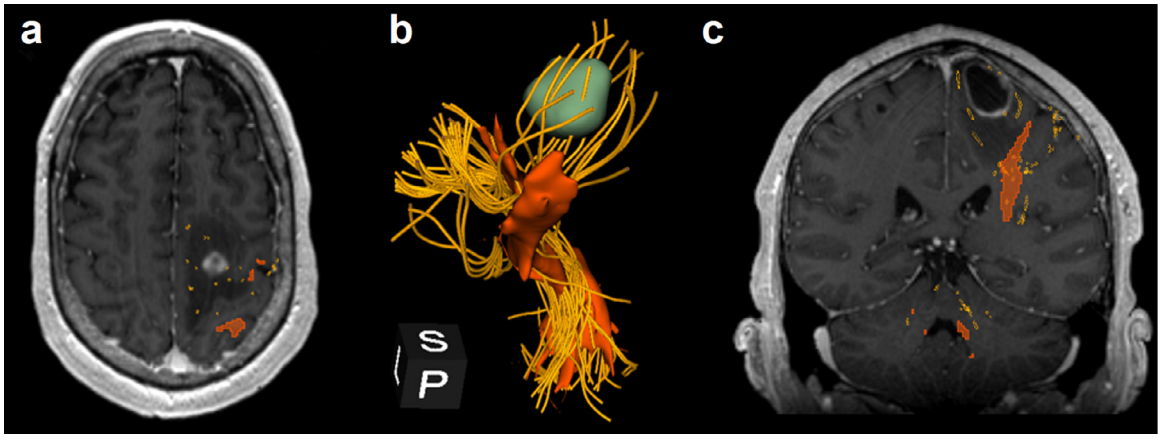

Fig. 7. Comparison of DTI tractography to advanced tractography using an unscented Kalman filter (UKF) in the same patient as in Fig. 5. (a) The corticospinal tract (CST) generated by DTI-based tractography (reddish-orange) and UKF (golden yellow). UKF tractography shows CST going through the edematous region around the tumor, whereas DTI tractography does not capture those peritumoral tracts. (b) The tractogram shows a 3D-reconstructions of the CST from DTI tractography (reddish-orange), using commercially available navigation software, and from UKF tractography (golden yellow), using the SlicerDMRI module in 3D Slicer. It is noteworthy that UKF tractography allows one to visualize CST innervating the lower extremities, upper extremities, and face (peripheral, extracerebral trajectories not shown). In contrast, DTI-based tractography shows only tracts from the same region of the motor cortex, likely corresponding to upper extremities. (c) Coronal, contrast-enhanced T_1-weighted MRI integrated with tractogram illustrates the two tractography techniques and the ability of advanced tractography to identify tracts in the edematous region of the peritumoral area.

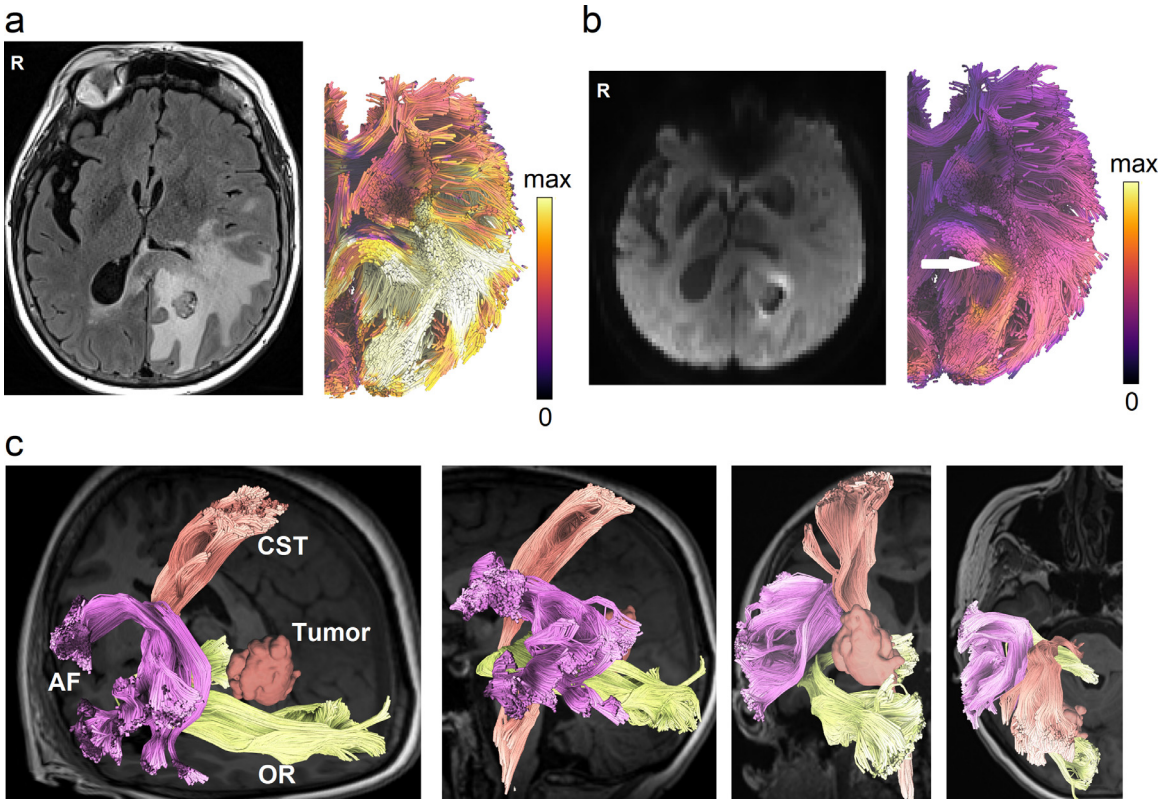

Fig. 8. Novel tractography approaches showing perilesional white matter pathways of a 65-year-old female patient with glioblastoma multiforme (GBM) to assist presurgical planning or postsurgical assessment. (a) Advanced tractography can be integrated with other imaging modalities to assist diagnostic and prognostic evaluation. The tractogram is color-coded by T_2/FLAIR to visualize pathways affected by peritumoral edema. (b) Tractograms can be color-coded according to cell densities estimated from restricted diffusion imaging (Yeh et al., 2017) to highlight tracts infiltrated by tumor cells (annotated by the white arrow). The results may inform the extent of surgical resection to achieve better surgical results. (c) Automated tractography maps the arcuate fasciculus (AF), corticospinal tract (CST), and optic radiation (OR) of the patient to facilitate presurgical planning. This new tractography approach uses prior anatomical information from a tractography atlas to identify white matter pathways, eliminate spurious tracks, and cluster tracks into anatomically defined bundles. This process can reduce the tedious manual placement of seed regions and can improve the test-retest reliability of tractography mapping.

For clinical groups already using DTI tractography, transition to beyond-DTI can be readily achieved by combining two sets of DTI data at different b-values. For example, one DTI acquisition can be acquired at a b-value of 1500 s/mm^2 at 30 directions, whereas another DTI acquisition can be subsequently acquired at a b-value of 3000 s/mm^2 at 60 directions. Both acquisitions should use the identical isotropic resolution and identical TE and TR. These two DTI data combined is a two-shell dataset that can be readily utilized by more advanced modeling methods mentioned above, including and not limited to GQI, MSMT-CSD, NODDI, and DKI. Combining two-shell protocol and beyond-DTI methods offers the potential to remove free water and minimize the effect of peritumoral edema. Furthermore, many tractography tools shared their applicable imaging protocol to encourage reproducible research and open science (Norton et al., 2017). We also shared our 12-minute grid scheme protocol at the DSI Studio website (http://dsi-studio.labsolver.org), which acquired 23 b-values at 258 directions to characterize a spectrum of restricted and non-restricted diffusion.

Challenges remain for future advanced tractography methods to address when mapping white matter in brain tumor patients. Currently, there is no standardization of dMRI tractography methods used by different institutions. For example, as mentioned in previous sections, studies have demonstrated considerable variability in fully reconstructing the pyramidal pathway among different approaches (Pujol et al., 2015; Schilling et al., 2020). Research has already demonstrated that operator-dependent effects such as the choice of regions (e.g., either seed regions or region of interest) can often affect tractography results (Radmanesh et al., 2015). Even the same tractography method implemented within different software environments can have a wide range of performance discrepancies (Maier-Hein et al., 2017; Schilling et al., 2021). Thus, reproducibility and standardization are critical challenges that must be overcome for tractography to gain further trust within the neurosurgery community. This issue is crucial in neurosurgical settings, where tractography errors can give clinicians incorrect information on the location of critical structures and could thus increase the risk of postoperative deficits for some patients (Duffau, 2014). One promising direction is automated tract identification for brain tumor patients (O'Donnell et al., 2017). Precisely, by using a tractography atlas, automated tractography can map white matter pathways in the eloquent areas to facilitate neurosurgical planning (Fig. 8c). Clinicians can specify tracts of interest to visualize their relationship to the lesion. This new tractography visualization approach can reduce the time needed for manual placement of regions, improve the reliability of pathway mapping, and potentially promote the future standardization of presurgical planning.

8. Tractography in patients with TBI

8.1. DTI tractography in TBI

DTI tractography has contributed substantially to our understanding of longitudinal TBI effects upon the connectome as a function of age (Irimia et al., 2015; Trotter et al., 2015), injury chronicity (Ewing-Cobbs et al., 2016), impact mechanism (Petrie et al., 2014; Tremblay et al., 2014), trauma severity (Ilvesmaki et al., 2014) and clin-

ical outcome (Yuh et al., 2014). Additionally, it has allowed scientists to study how white matter structures (Wright et al., 2016), cognitive abilities (Caeyenberghs et al., 2014; Calvillo and Irimia, 2020), and connectome properties (Fagerholm et al., 2015) are differentially vulnerable to TBI under a variety of conditions. Studies have combined standard tractography with sophisticated biomechanical models to identify structural connectome regions most vulnerable to mild injury (Sullivan et al., 2015; Zhao et al., 2017). Furthermore, DTI tractography has been leveraged to serve as a reliable surrogate biomarker for vasogenic edema in peri-hemorrhagic TBI regions (Yang et al., 2017) to identify post-traumatic blood-brain barrier permeability changes and to quantify abnormal iron deposition within the brain parenchyma (Wright et al., 2016). These critical contributions give rise to detectable cerebral microbleeds in susceptibility-weighted imaging suggesting traumatic axonal injury and blood-brain barrier breakdown (Irimia et al., 2018), which are relevant for mild traumatic brain injury (mTBI) diagnosis in the absence of other imaging findings (Rostowsky et al., 2018). Tractography has also served as a welcome adjuvant to electrophysiological methods for mapping functional connectome properties, the loci of post-traumatic epilepsy, and related functional manifestations of post-traumatic sequelae (Irimia et al., 2013; Irimia and Van Horn, 2015a).

8.2. Limitations of DTI tractography in TBI

Despite the breadth and value of DTI studies to characterize TBI sequelae within the connectome, the utility and interpretation of DTI measures in TBI remain equivocal (Van Horn et al., 2017). To a substantial extent, these challenges echo those described in the previous sections. Whereas FA is commonly assumed to decrease after mTBI, a sizeable number of studies have concluded otherwise (Arfanakis et al., 2002; Inglese et al., 2005; Kinnunen et al., 2011; Kumar et al., 2009; Lipton et al., 2009; Lo et al., 2009; Miles et al., 2008; Toth et al., 2013). This debate has not been settled even after accounting for the effects of confounds such as injury chronicity, age at injury, publication date, and methodological differences across studies (Dodd et al., 2014; Eierud et al., 2014). Furthermore, FA has been frequently associated with white matter damage in TBI because its mathematically related metrics, axial diffusivity (AD) and radial diffusivity (RD), are considered to be surrogate markers of axonal and myelin damage, respectively (Song et al., 2003; Song et al., 2002; Song et al., 2005; Sun et al., 2006; Winklewski et al., 2018). This relative consensus persists, although such measures remain challenging to interpret in the presence of inflammation and edema. For example, AD may decrease during acute demyelination in the presence of axonal edema and microglial activation, but not during chronic demyelination of the connectome (Lodygensky et al., 2010). Similarly, RD increases chronically in demyelinating conditions unless edema is present, in which case RD does not appear to change significantly (Xie et al., 2010). Thus, because brain trauma-related inflammation and scarring can substantially change white matter structure across time, the interpretation of AD, RD, and FA in TBI is challenging as it depends on factors like lesion content and temporal evolution. Thus, additional research is needed to understand how inflammation, hemorrhage, axotomy, axonal injury, and demyelination interact post-traumatically to affect both the connectome and DTI measures (Armstrong et al., 2016). Some investigators have even proposed that standard DTI tractography is insufficiently reliable for interpreting TBI pathology in the presence of such complex cellular phenomena (Winklewski et al., 2018) and that more sophisticated techniques should be used (Cross and Song, 2017).

Another challenge of using DTI tractography in TBI is that many tensor assumptions may be violated in the presence of traumatic axonal injury. This latter phenomenon involves axonal shearing, twisting, or swelling that affects cellular morphology. The ensuing dysregulation of homeostatic calcium transmembrane gradients compromises cellular permeability and exacerbates morphological alterations in the axonal microstructure. These changes are poorly captured by DTI, particularly in the ubiquitous scenario where vasogenic and cytotoxic edema compete in the extent to which they dysregulate cellular function and tissue integrity. In response to such concerns, NODDI and *q*-space metrics—which can quantify intra-axonal volume fractions—have been proposed as techniques that provide sensitive and specific biomarkers of post-traumatic white matter disruption, macroscale tissue alterations, or cognitive deficits associated with TBI sequelae (Wu et al., 2018). Nevertheless, while relying on electron microscopy data to validate FA values and DTI streamline orientations in a murine TBI model, Salo et al. found that the orientations of DTI tractography streamlines can accurately reflect electron microscopy (EM)-derived white matter fiber orientations (Salo et al., 2018). However, the extension of such findings to humans may be problematic because many tractography validation studies in animals have used spatial resolutions more than an order of magnitude higher than typical human studies (Salo et al., 2018).

FAs and DTI streamline orientations have been validated only for a limited range of lesion content types. Subsequent tractography validation studies involving the integration of histology, structural MRI, and GQI have led to the proposal of additional, novel connectome integrity metrics that may be superior to traditional measures like FA (Gangolli et al., 2017). Additional validation studies are much needed to establish further how well DTI and beyond-DTI findings can capture the accurate underlying presentation of TBI and its impact upon the mesoscale connectome, topics which remain understudied (Laitinen et al., 2015).

8.3. Advanced tractography in TBI

Hoping to overcome the current drawbacks of DTI as used in TBI studies, some scientists have proposed estimating fiber orientation distributions directly from advanced acquisitions and using spherical deconvolution measures such as apparent fiber density track-weighted imaging to characterize post-traumatic connectome alterations (Wright et al., 2017). Other scientists advocate using diffuse kurtosis imaging (DKI) and related methods to obtain novel insights into post-traumatic connectome reorganization (Hansen and Jespersen, 2017). More recently, tractography approaches have been integrated with functional MRI (fMRI)-derived blood oxygenation level-dependent (BOLD) models and with positron emission tomography (PET) (Wooten et al., 2019) or magnetic resonance spectroscopy (Li et al., 2017; Maudsley et al., 2015; Narayana et al., 2015). The multimodally datasets could establish the relationship between TBI and other neurological conditions and forecast post-traumatic risk for further cognitive deficits based on connectomic data (Irimia et al., 2020). This integration has assisted some researchers in gaining insights into the relationship between (a) tractography streamline properties and functional correlation metrics and between (b) clinical variables of neurodegeneration (like tau protein aggregate burden) and measures of metabolic damage and oxidative stress. Wooten et al. (2019) found that DTI-derived tractography measures traditionally associated with white matter integrity are related to fMRI functional correlations and tauopathies in complex ways, which may require substantial additional research to disentangle. Although DTI-derived tractography measures of post-traumatic white matter integrity loss and connectome degradation may translate into an elevated tau-aggregate burden, they may also be associated with higher—rather than lower— functional correlations mediated by white matter connections exhibiting such burden (Irimia and Van Horn, 2015b). More recent findings suggest that the relationship between oxygen consumption in neural tissue and white matter architecture parameters provided by DTI tractography remains woefully incomplete in TBI conditions (Armstrong et al., 2016; Wooten et al., 2019; Wright et al., 2016). Other novel tractography modalities like *differential tractography* (Yeh et al., 2019) may also provide new ways to investigate the injury mechanisms by mapping longitudinal alterations in brain connectivity (Fig. 9). Nevertheless, systematic testing and validation of this and many other DTI models remain to be undertaken, and future stud-

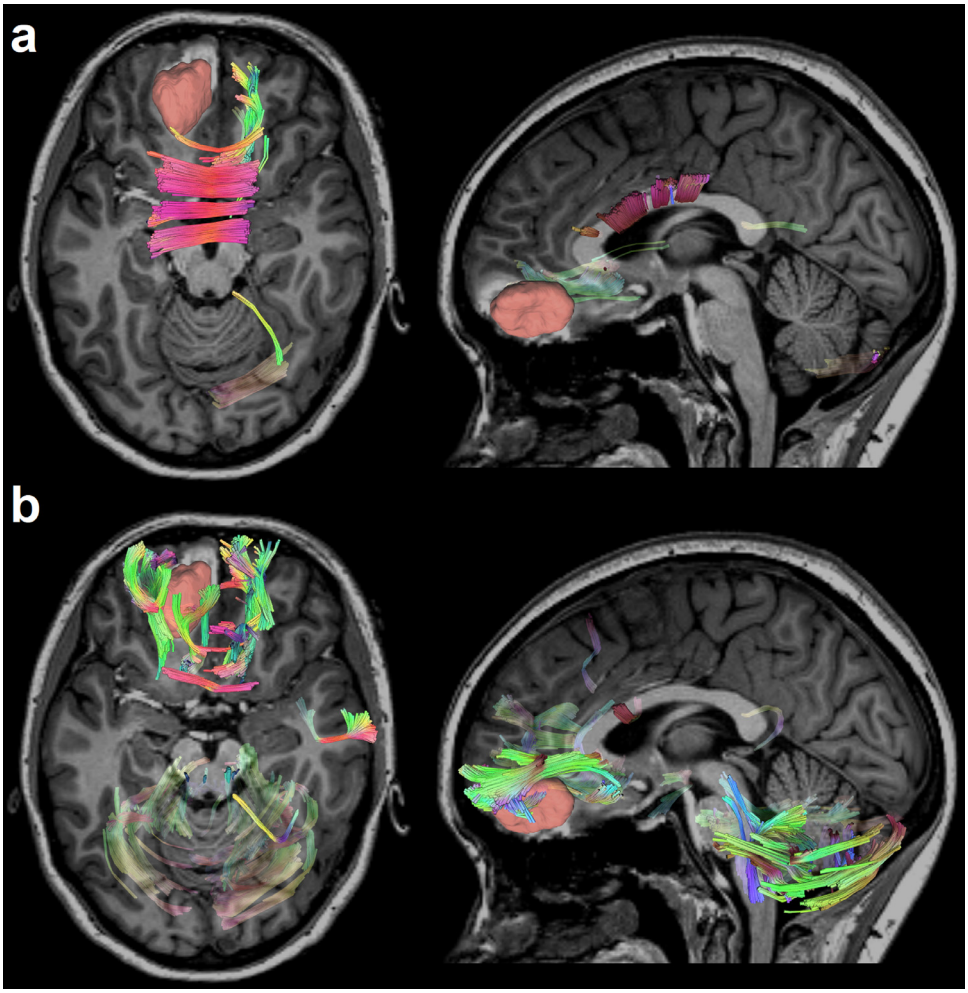

Fig. 9. *Differential tractography* of a 19-year-old female TBI patient highlighting the exact segments of neuronal pathways with anisotropy changes between a baseline scan acquired acutely (i.e., within a week after injury) and a follow-up scan (approximately 6 months post-TBI). The patient features a relatively large primary lesion located in the left orbitofrontal cortex, which is particularly vulnerable to TBI. Differential tractography (Yeh et al., 2019) tracks the precise segments of pathways exhibiting (a) FA decreases of more than 5% relative to the acute baseline and (b) quantitative anisotropy (QA) decreases of more than 15% relative to the same baseline. Directional coding is used to color the tractogram (left-right: red; anterior-posterior: green; superior-inferior: blue). The results reveal perilesional tracts and the genu of the corpus callosum (CC), which is the CC portion closest to the primary lesion (red). Traumatic axonal injury (TAI) of the CC is prevalent in TBI and can be explained by the interaction of TBI kinematics with the biomechanics of cerebral displacement within the cranial cavity (Hill et al., 2016). The decrease in cerebellar FA and QA is consistent with previous findings, according to which cerebellar volume and connectivity are both frequently and substantially affected by moderate and severe TBI regardless of primary injury location (Spanos et al., 2007). Although this fact is well documented (Caeyenberghs et al., 2011; Irimia et al., 2012; Park et al., 2006), its causal mechanisms are poorly understood and may be related to cerebellar involvement in motor coordination, control, and other brain functions. These functions are frequently and substantially impacted both by the primary injury and by decreases in TBI patients' abilities to carry out daily living activities as they recover. New tractography modalities like differential tractography may offer novel strategies to investigate white matter pathways and to answer outstanding questions in TBI research.

ies should also seek to (a) ascertain the validity of both established and novel diffusion MRI measures upon which tractography is reliant and to (b) resolve the complicated relationship between multimodal metrics provided by MRI, electroencephalography (EEG), magnetoencephalography (MEG), PET, and temporal connectome dynamics.

9. Prospect of tractography development

9.1. Automated tractography

Because recent tractography challenges have highlighted the inherent limitations of dMRI, strategies resorting to external information independent of this technique have gained more attention (Schilling et al., 2019b). One recent trend is to utilize a brain parcellation or tractography atlas to inform automated tractography, thus resulting in new tracking approaches or post-tracking scrutiny routines (Garyfallidis et al., 2018; Guevara et al., 2012; O'Donnell and Westin, 2007; O'Donnell et al., 2017; Rheault et al., 2019; Warrington et al., 2020; Wassermann et al., 2016; Wasserthal et al., 2018; Yeatman et al., 2012; Yeh, 2020; Yendiki et al., 2011; Zollei et al., 2019). These methods often use prior anatomical information to identify tracts and simultaneously to reject spurious connections while improving anatomic accuracy. Automated tractography also eliminates human subjectivity in fiber tracking and vastly improves the reproducibility of fiber tracking. Furthermore, a study using repeat scans has shown that automated tractography can achieve high test-retest reliability when mapping association pathways (Fig. 10a) (Yeh, 2020). Although the accuracy and consistency between methods remain an issue, the high reproducibility within automated tractography methods can significantly improve their clinical utilities, where reliable results are prerequisites for further applications.

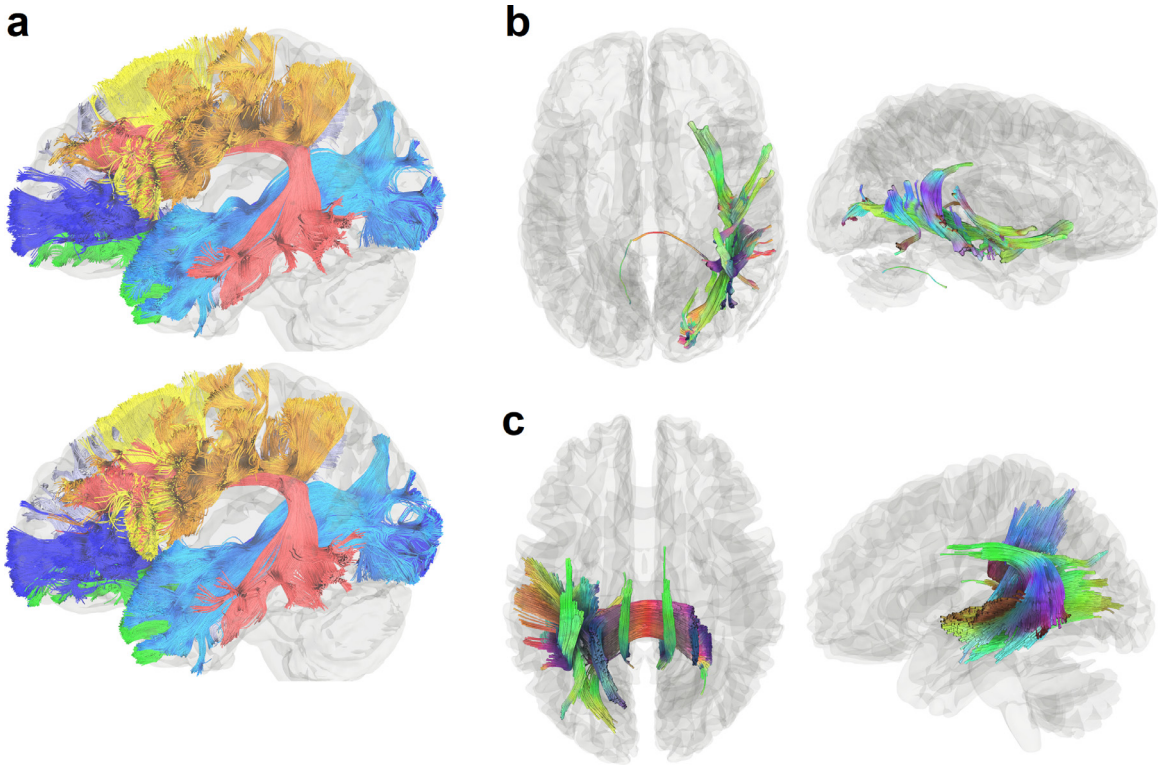

Fig. 10. Prospects of novel tractography developments to improve reliability and to explore the potential of new clinical applications. (a) Automated tractography from repeat MRI scans of the same healthy young adult subject shows high reproducibility in mapping human association pathways. Novel developments in automated tractography can mitigate quality variations due to human error and achieve better test-retest reliability. (b) Differential tractography is a new tractography modality that detects between-scan differences by tracking pathways with decreased anisotropy or any metrics. Here, differential tractography maps the precise segments of pathways with neuronal property changes by comparing the preoperative and postoperative scans of a 51-year-old male epileptic patient after anterior temporal lobectomy (Yeh et al., 2019). The affected tracts span beyond the operation location. Directional color coding is used to color the tractogram (left-right: red, anterior-posterior: green, superior-inferior: blue). (c) Correlational tractography shows connections correlated with aphasia severity in a stroke study with participants ranged from 31 to 82 years of age (Hula et al., 2020). The tractogram is colored by directional colors. This new tractography modality tracks correlation along white matter pathways to map the precise segment of connections correlated with the study variable (e.g., aphasia severity). It can be used to probe the circuit mechanism underlying brain dysfunction in neurological disorders.

9.2. New tractography modalities

Another prospect of tractography is leveraging new tractography modalities to overcome existing limitations and enable novel clinical applications. One known limitation of tractography is that streamline counts do not have biological meaning (Johansen-Berg and Behrens, 2006; Jones and Cercignani, 2010; O'Donnell and Pasternak, 2014), and track trajectories are not informative for many brain diseases. This is because a subtle change in anisotropy or diffusivity does not necessarily imply a lower streamline count unless the anisotropy value plunges below the termination threshold. This anisotropy threshold can be a value as low as 0.1 for FA, and thus subtle changes above this threshold are not typically detectable by standard tractography. In attempting to address this limitation, studies have imbued tractography with diffusion information to closely associate the streamline counts with neuronal changes (Girard et al., 2017; Smith et al., 2013). Such enhanced tractography could be used in diagnostic or prognostic evaluation of brain diseases and other pathological conditions without resorting to diffusion metrics (Conti et al., 2017; Ziegler et al., 2014). These approaches can be instrumental in TBI, where axonal counts may decrease or increase post-injury depending on whether individual anatomic white matter connections are weakened or strengthened as the brain recovers.

More recently, a new tractography modality called *differential tractography* was introduced to map the exact segments of white matter tracts with decreased anisotropy (Yeh et al., 2019). The method included an additional termination criterion to the fiber tracking algorithm, such that the resulting differential tractography could be used as a whole-brain screening tool to reveal pathways with subtle anisotropy differences in longitudinal studies (Fig. 10b). For group studies, a similar paradigm can be followed to track correlation along pathways and, thereby, to produce *correlational tractography* (Fig. 10c), whose results can be compared statistically using permutation tests (Yeh et al., 2016). Studies have shown that correlational tractography can reveal the structural mechanism behind brain function and dysfunction (Hula et al., 2020; Sanchez-Catasus et al., 2020). These new modalities warrant additional research to examine their clinical values as novel track-based imaging biomarkers.

Credit author statement

FY, AI, DBC, and AJG wrote the manuscript.

Data and code

The HCP data are available at https://db.humanconnectome.org. The Penthera 3T data are available at https://zenodo.org/record/2602049. The Traveling adults subjects data are available at https://figshare.com/articles/dataset/Multicenter_dataset_of_multishell_diffusion_magnetic_resonance_imaging_in_healthy_traveling_adults_with_identical_setting/8851955. The MRI data for clinical patients are not available to the public due to privacy issues. DSI Studio is available at http://dsi-studio.labsolver.org with

source code available at https://github.com/frankyeh/DSI-Studio. SlicerDMRI is available at http://dmri.slicer.org/

Declaration of Competing Interest

FY, AI, DBC, and AJG declare that this review was conducted in the absence of any commercial or financial relationship that could be construed as a potential conflict of interest.

Acknowledgment

AI is supported by NIH grant R01 NS 100973, by DoD award W81-XWH-1810413, and by a USC Hanson-Thorell Research Scholarship. AJG is supported by NIH grants U01 CA 199459 and P41 EB 015898, and by the Jennifer Oppenheimer Cancer Research Initiative. FY's work is partly supported by the Alba Tull Center for Neuro Imaging and Therapeutics funded by the Tull Family Foundation

References

Abhinav, K., Yeh, F.C., Mansouri, A., Zadeh, G., Fernandez-Miranda, J.C., 2015. High--definition fiber tractography for the evaluation of perilesional white matter tracts in high-grade glioma surgery. Neuro. Oncol. 17, 1199–1209.

Aganj, I., Lenglet, C., Sapiro, G., Yacoub, E., Ugurbil, K., Harel, N., 2010. Reconstruction of the orientation distribution function in single- and multiple-shell q-ball imaging within constant solid angle. Magn. Reson. Med. 64, 554–566.

Alexander, A.L., Hasan, K.M., Lazar, M., Tsuruda, J.S., Parker, D.L., 2001. Analysis of partial volume effects in diffusion-tensor MRI. Magn. Reson. Med. 45, 770–780.

Alexopoulos, G., Cikla, U., El Tecle, N., Kulkarni, N., Pierson, M., Mercier, P., Kemp, J., Coppens, J., Mahmoud, S., Sehi, M., Bucholz, R., Abdulrauf, S., 2019. The value of white matter tractography by diffusion tensor imaging in altering a neurosurgeon's operative plan. World Neurosurg. 132, e305–e313.

Aliotta, E., Moulin, K., Ennis, D.B., 2018. Eddy current-nulled convex optimized diffusion encoding (EN-CODE) for distortion-free diffusion tensor imaging with short echo times. Magn. Reson. Med. 79, 663–672.

Andersson, J.L., Skare, S., Ashburner, J., 2003. How to correct susceptibility distortions in spin-echo echo-planar images: application to diffusion tensor imaging. Neuroimage 20, 870–888.

Andersson, J.L., Sotiropoulos, S.N., 2015. Non-parametric representation and prediction of single- and multi-shell diffusion-weighted MRI data using Gaussian processes. Neuroimage 122, 166–176.

Andersson, J.L.R., Sotiropoulos, S.N., 2016. An integrated approach to correction for off-resonance effects and subject movement in diffusion MR imaging. Neuroimage 125, 1063–1078.

Arfanakis, K., Haughton, V.M., Carew, J.D., Rogers, B.P., Dempsey, R.J., Meyerand, M.E., 2002. Diffusion tensor MR imaging in diffuse axonal injury. AJNR Am. J. Neuroradiol. 23, 794–802.

Armstrong, R.C., Mierzwa, A.J., Marion, C.M., Sullivan, G.M., 2016. White matter involvement after TBI: Clues to axon and myelin repair capacity. Exp. Neurol. 328–333 275 Pt 3.

Assaf, Y., Basser, P.J., 2005. Composite hindered and restricted model of diffusion (CHARMED) MR imaging of the human brain. Neuroimage 27, 48–58.

Assaf, Y., Freidlin, R.Z., Rohde, G.K., Basser, P.J., 2004. New modeling and experimental framework to characterize hindered and restricted water diffusion in brain white matter. Magn. Reson. Med. 52, 965–978.

Avesani, P., McPherson, B., Hayashi, S., Caiafa, C.F., Henschel, R., Garyfallidis, E., Kitchell, L., Bullock, D., Patterson, A., Olivetti, E., Sporns, O., Saykin, A.J., Wang, L., Dinov, I., Hancock, D., Caron, B., Qian, Y., Pestilli, F., 2019. The open diffusion data derivatives, brain data upcycling via integrated publishing of derivatives and reproducible open cloud services. Sci. Data 6, 69.

Basser, P.J., Mattiello, J., LeBihan, D., 1994. Estimation of the effective self-diffusion tensor from the NMR spin echo. J. Magn. Reson. B 103, 247–254.

Basser, P.J., Pajevic, S., Pierpaoli, C., Duda, J., Aldroubi, A., 2000. In vivo fiber tractography using DT-MRI data. Magn. Reson. Med. 44, 625–632.

Bastiani, M., Cottaar, M., Fitzgibbon, S.P., Suri, S., Alfaro-Almagro, F., Sotiropoulos, S.N., Jbabdi, S., Andersson, J.L.R., 2019. Automated quality control for within and between studies diffusion MRI data using a non-parametric framework for movement and distortion correction. Neuroimage 184, 801–812.

Becker, D., Scherer, M., Neher, P., Jungk, C., Jesser, J., Pflüger, I., Brinster, R., Bendszus, M., Bruckner, T., Maier-Hein, K., 2020. Going Beyond Diffusion Tensor Imaging Tractography in Eloquent Glioma Surgery–High-Resolution Fiber Tractography: Q-Ball or Constrained Spherical Deconvolution? World Neurosurg. 134, e596–e609.

Behrens, T.E., Johansen-Berg, H., Woolrich, M.W., Smith, S.M., Wheeler-Kingshott, C.A., Boulby, P.A., Barker, G.J., Sillery, E.L., Sheehan, K., Ciccarelli, O., Thompson, A.J., Brady, J.M., Matthews, P.M., 2003a. Non-invasive mapping of connections between human thalamus and cortex using diffusion imaging. Nat. Neurosci. 6, 750–757.

Behrens, T.E., Woolrich, M.W., Jenkinson, M., Johansen-Berg, H., Nunes, R.G., Clare, S., Matthews, P.M., Brady, J.M., Smith, S.M., 2003b. Characterization and propagation of uncertainty in diffusion-weighted MR imaging. Magn. Reson. Med. 50, 1077–1088.

Breuer, F.A., Blaimer, M., Heidemann, R.M., Mueller, M.F., Griswold, M.A., Jakob, P.M., 2005. Controlled aliasing in parallel imaging results in higher acceleration (CAIPIRINHA) for multi-slice imaging. Magn. Reson. Med. 53, 684–691.

Butts, K., Riederer, S.J., Ehman, R.L., Thompson, R.M., Jack, C.R., 1994. Interleaved echo planar imaging on a standard MRI system. Magn. Reson. Med. 31, 67–72.

Caeyenberghs, K., Leemans, A., Geurts, M., Linden, C.V., Smits-Engelsman, B.C., Sunaert, S., Swinnen, S.P., 2011. Correlations between white matter integrity and motor function in traumatic brain injury patients. Neurorehabil. Neural Repair 25, 492–502.

Caeyenberghs, K., Leemans, A., Leunissen, I., Gooijers, J., Michiels, K., Sunaert, S., Swinnen, S.P., 2014. Altered structural networks and executive deficits in traumatic brain injury patients. Brain Struct. Funct. 219, 193–209.

Cai, L.Y., Yang, Q., Hansen, C.B., Nath, V., Ramadass, K., Johnson, G.W., Conrad, B.N., Boyd, B.D., Begnoche, J.P., Beason-Held, L.L., Shafer, A.T., Resnick, S.M., Taylor, W.D., Price, G.R., Morgan, V.L., Rogers, B.P., Schilling, K.G., Landman, B.A., 2021. PreQual: An automated pipeline for integrated preprocessing and quality assurance of diffusion weighted MRI images. Magn. Reson. Med. 86, 456–470.

Callaghan, P.T., 1991. Principles of Nuclear Magnetic Resonance Microscopy. Oxford University Press.

Calvillo, M., Irimia, A., 2020. Neuroimaging and psychometric assessment of mild cognitive impairment after traumatic brain injury. Front. Psychol. 11, 1423.

Celtikci, P., Fernandes-Cabral, D.T., Yeh, F.C., Panesar, S.S., Fernandez-Miranda, J.C., 2018. Generalized q-sampling imaging fiber tractography reveals displacement and infiltration of fiber tracts in low-grade gliomas. Neuroradiology 60, 267–280.

Chen, Z., Tie, Y., Olubiyi, O., Rigolo, L., Mehrtash, A., Norton, I., Pasternak, O., Rathi, Y., Golby, A.J., O'Donnell, L.J., 2015a. Reconstruction of the arcuate fasciculus for surgical planning in the setting of peritumoral edema using two-tensor unscented Kalman filter tractography. NeuroImage: Clinical 7, 815–822.

Chen, Z., Tie, Y., Olubiyi, O., Rigolo, L., Mehrtash, A., Norton, I., Pasternak, O., Rathi, Y., Golby, A.J., O'Donnell, L.J., 2015b. Reconstruction of the arcuate fasciculus for surgical planning in the setting of peritumoral edema using two-tensor unscented Kalman filter tractography. Neuroimage Clin. 7, 815–822.

Cho, K.H., Yeh, C.H., Tournier, J.D., Chao, Y.P., Chen, J.H., Lin, C.P., 2008. Evaluation of the accuracy and angular resolution of q-ball imaging. Neuroimage 42, 262–271.

Christiaens, D., Reisert, M., Dhollander, T., Sunaert, S., Suetens, P., Maes, F., 2015. Global tractography of multi-shell diffusion-weighted imaging data using a multi-tissue model. Neuroimage 123, 89–101.

Cieslak, M., Cook, P.A., He, X., Yeh, F.C., Dhollander, T., Adebimpe, A., Aguirre, G.K., Bassett, D.S., Betzel, R.F., Bourque, J., Cabral, L.M., Davatzikos, C., Detre, J.A., Earl, E., Elliott, M.A., Fadnavis, S., Fair, D.A., Foran, W., Fotiadis, P., Garyfallidis, E., Giesbrecht, B., Gur, R.C., Gur, R.E., Kelz, M.B., Keshavan, A., Larsen, B.S., Luna, B., Mackey, A.P., Milham, M.P., Oathes, D.J., Perrone, A., Pines, A.R., Roalf, D.R., Richie-Halford, A., Rokem, A., Sydnor, V.J., Tapera, T.M., Tooley, U.A., Vettel, J.M., Yeatman, J.D., Grafton, S.T., Satterthwaite, T.D., 2021. QSIPrep: an integrative platform for preprocessing and reconstructing diffusion MRI data. Nat. Methods 18, 775–778.

Coenen, V.A., Allert, N., Madler, B., 2011. A role of diffusion tensor imaging fiber tracking in deep brain stimulation surgery: DBS of the dentato-rubro-thalamic tract (drt) for the treatment of therapy-refractory tremor. Acta Neurochir. (Wien) 153, 1579–1585 discussion 1585.

Coenen, V.A., Krings, T., Mayfrank, L., Polin, R.S., Reinges, M.H., Thron, A., Gilsbach, J.M., 2001. Three-dimensional visualization of the pyramidal tract in a neuronavigation system during brain tumor surgery: first experiences and technical note. Neurosurgery 49, 86–92 discussion 92-83.

Conti, E., Mitra, J., Calderoni, S., Pannek, K., Shen, K.K., Pagnozzi, A., Rose, S., Mazzotti, S., Scelfo, D., Tosetti, M., Muratori, F., Cioni, G., Guzzetta, A., 2017. Network over-connectivity differentiates autism spectrum disorder from other developmental disorders in toddlers: a diffusion MRI study. Hum. Brain Mapp. 38, 2333–2344.

Cottaar, M., Bastiani, M., Boddu, N., Glasser, M.F., Haber, S., van Essen, D.C., Sotiropoulos, S.N., Jbabdi, S., 2020. Modelling white matter in gyral blades as a continuous vector field. Neuroimage 227, 117693.

Craddock, R.C., Jbabdi, S., Yan, C.G., Vogelstein, J.T., Castellanos, F.X., Di Martino, A., Kelly, C., Heberlein, K., Colcombe, S., Milham, M.P., 2013. Imaging human connectomes at the macroscale. Nat. Methods 10, 524–539.

Cross, A.H., Song, S.K., 2017. A new imaging modality to non-invasively assess multiple sclerosis pathology. J. Neuroimmunol. 304, 81–85.

Dell'acqua, F., Scifo, P., Rizzo, G., Catani, M., Simmons, A., Scotti, G., Fazio, F., 2009. A modified damped Richardson-Lucy algorithm to reduce isotropic background effects in spherical deconvolution. Neuroimage 49, 1446–1458.

Descoteaux, M., Angelino, E., Fitzgibbons, S., Deriche, R., 2007. Regularized, fast, and robust analytical Q-ball imaging. Magn. Reson. Med. 58, 497–510.

Descoteaux, M., Deriche, R., Knosche, T.R., Anwander, A., 2009. Deterministic and probabilistic tractography based on complex fibre orientation distributions. IEEE Trans. Med. Imaging 28, 269–286.

Dodd, A.B., Epstein, K., Ling, J.M., Mayer, A.R., 2014. Diffusion tensor imaging findings in semi-acute mild traumatic brain injury. J. Neurotrauma 31, 1235–1248.

Duffau, H., 2014. The dangers of magnetic resonance imaging diffusion tensor tractography in brain surgery. World Neurosurg. 81, 56–58.

Eierud, C., Craddock, R.C., Fletcher, S., Aulakh, M., King-Casas, B., Kuehl, D., LaConte, S.M., 2014. Neuroimaging after mild traumatic brain injury: review and meta–analysis. Neuroimage Clin. 4, 283–294.

Ewing-Cobbs, L., Johnson, C.P., Juranek, J., DeMaster, D., Prasad, M., Duque, G., Kramer, L., Cox, C.S., Swank, P.R., 2016. Longitudinal diffusion tensor imaging after pediatric traumatic brain injury: impact of age at injury and time since injury on pathway integrity. Hum. Brain Mapp. 37, 3929–3945.

Fagerholm, E.D., Hellyer, P.J., Scott, G., Leech, R., Sharp, D.J., 2015. Disconnection

of network hubs and cognitive impairment after traumatic brain injury. Brain 138, 1696–1709.
Fan, Q., Nummenmaa, A., Witzel, T., Zanzonico, R., Keil, B., Cauley, S., Polimeni, J.R., Tisdall, D., Van Dijk, K.R., Buckner, R.L., Wedeen, V.J., Rosen, B.R., Wald, L.L., 2014. Investigating the capability to resolve complex white matter structures with high b–value diffusion magnetic resonance imaging on the MGH-USC Connectom scanner. Brain Connect. 4, 718–726.
Farquharson, S., Tournier, J.-D., Calamante, F., Fabinyi, G., Schneider-Kolsky, M., Jackson, G.D., Connelly, A., 2013. White matter fiber tractography: why we need to move beyond DTI. J. Neurosurg. 118, 1367–1377.
Fekonja, L., Wang, Z., Bahrend, I., Rosenstock, T., Rosler, J., Wallmeroth, L., Vajkoczy, P., Picht, T., 2019. Manual for clinical language tractography. Acta Neurochir. (Wien) 161, 1125–1137.
Fekonja, L.S., Wang, Z., Aydogan, D.B., Roine, T., Engelhardt, M., Dreyer, F.R., Vajkoczy, P., Picht, T., 2020. Detecting corticospinal tract impairment in tumor patients with fiber density and tensor-based metrics. Front. Oncol. 10, 622358.
Fernandez-Miranda, J.C., Pathak, S., Engh, J., Jarbo, K., Verstynen, T., Yeh, F.C., Wang, Y., Mintz, A., Boada, F., Schneider, W., Friedlander, R., 2012. High-definition fiber tractography of the human brain: neuroanatomical validation and neurosurgical applications. Neurosurgery 71, 430–453.
Fieremans, E., Jensen, J.H., Helpern, J.A., 2011. White matter characterization with diffusional kurtosis imaging. Neuroimage 58, 177–188.
Fillard, P., Descoteaux, M., Goh, A., Gouttard, S., Jeurissen, B., Malcolm, J., Ramirez–Manzanares, A., Reisert, M., Sakaie, K., Tensaouti, F., 2011. Quantitative evaluation of 10 tractography algorithms on a realistic diffusion MR phantom. Neuroimage 56, 220–234.
Finsterbusch, J., 2009. Eddy-current compensated diffusion weighting with a single refocusing RF pulse. Magn. Reson. Med. 61, 748–754.
Gangolli, M., Holleran, L., Hee Kim, J., Stein, T.D., Alvarez, V., McKee, A.C., Brody, D.L., 2017. Quantitative validation of a nonlinear histology-MRI coregistration method using generalized Q-sampling imaging in complex human cortical white matter. Neuroimage 153, 152–167.
Garyfallidis, E., Cote, M.A., Rheault, F., Sidhu, J., Hau, J., Petit, L., Fortin, D., Cunanne, S., Descoteaux, M., 2018. Recognition of white matter bundles using local and global streamline-based registration and clustering. Neuroimage 170, 283–295.
Genc, S., Tax, C.M.W., Raven, E.P., Chamberland, M., Parker, G.D., Jones, D.K., 2020. Impact of b-value on estimates of apparent fibre density. Hum. Brain Mapp. 41, 2583–2595.
Girard, G., Daducci, A., Petit, L., Thiran, J.P., Whittingstall, K., Deriche, R., Wassermann, D., Descoteaux, M., 2017. AxTract: Toward microstructure informed tractography. Hum. Brain Mapp. 38, 5485–5500.
Glasser, M.F., Rilling, J.K., 2008. DTI tractography of the human brain's language pathways. Cerebral Cortex 18, 2471–2482.
Golby, A.J., Kindlmann, G., Norton, I., Yarmarkovich, A., Pieper, S., Kikinis, R., 2011. Interactive diffusion tensor tractography visualization for neurosurgical planning. Neurosurgery 68, 496–505.
Gong, S., Zhang, F., Norton, I., Essayed, W.I., Unadkat, P., Rigolo, L., Pasternak, O., Rathi, Y., Hou, L., Golby, A.J., 2018. Free water modeling of peritumoral edema using multi-fiber tractography: application to tracking the arcuate fasciculus for neurosurgical planning. PLoS One 13, e0197056.
Grisot, G., Haber, S.N., Yendiki, A., 2021. Diffusion MRI and anatomic tracing in the same brain reveal common failure modes of tractography. Neuroimage, 118300.
Guevara, P., Duclap, D., Poupon, C., Marrakchi-Kacem, L., Fillard, P., Le Bihan, D., Leboyer, M., Houenou, J., Mangin, J.F., 2012. Automatic fiber bundle segmentation in massive tractography datasets using a multi-subject bundle atlas. Neuroimage 61, 1083–1099.
Guo, F., de Luca, A., Parker, G., Jones, D.K., Viergever, M.A., Leemans, A., Tax, C.M.W., 2021. The effect of gradient nonlinearities on fiber orientation estimates from spherical deconvolution of diffusion magnetic resonance imaging data. Hum. Brain Mapp. 42, 367–383.
Hansen, B., Jespersen, S.N., 2017. Recent developments in fast kurtosis imaging. Front. Phys. 5.
Hansen, C.B., Nath, V., Hainline, A.E., Schilling, K.G., Parvathaneni, P., Bayrak, R.G., Blaber, J.A., Irfanoglu, O., Pierpaoli, C., Anderson, A.W., Rogers, B.P., Landman, B.A., 2019. Characterization and correlation of signal drift in diffusion weighted MRI. Magn. Reson. Imaging 57, 133–142.
Henderson, F., Abdullah, K.G., Verma, R., Brem, S., 2020. Tractography and the connectome in neurosurgical treatment of gliomas: the premise, the progress, and the potential. Neurosurg. Focus 48, E6.
Hervey-Jumper, S.L., Berger, M.S., 2019. Evidence for improving outcome through extent of resection. Neurosurg. Clin. N. Am. 30, 85–93.
Hill, C.S., Coleman, M.P., Menon, D.K., 2016. Traumatic axonal injury: mechanisms and translational opportunities. Trends Neurosci. 39, 311–324.
Hoefnagels, F.W., De Witt Hamer, P., Sanz-Arigita, E., Idema, S., Kuijer, J.P., Pouwels, P.J., Barkhof, F., Vandertop, W.P., 2014. Differentiation of edema and glioma infiltration: proposal of a DTI-based probability map. J. Neurooncol. 120, 187–198.
Holdsworth, S.J., Skare, S., Newbould, R.D., Guzmann, R., Blevins, N.H., Bammer, R., 2008. Readout-segmented EPI for rapid high resolution diffusion imaging at 3 T. Eur. J. Radiol. 65, 36–46.
Hui, E.S., Cheung, M.M., Chan, K.C., Wu, E.X., 2010. B-value dependence of DTI quantitation and sensitivity in detecting neural tissue changes. Neuroimage 49, 2366–2374.
Hula, W.D., Panesar, S., Gravier, M.L., Yeh, F.C., Dresang, H.C., Dickey, M.W., Fernandez-Miranda, J.C., 2020. Structural white matter connectometry of word production in aphasia: an observational study. Brain 143, 2532–2544.
Ilvesmaki, T., Luoto, T.M., Hakulinen, U., Brander, A., Ryymin, P., Eskola, H., Iverson, G.L., Ohman, J., 2014. Acute mild traumatic brain injury is not associated with white matter change on diffusion tensor imaging. Brain 137, 1876–1882.
Inglese, M., Makani, S., Johnson, G., Cohen, B.A., Silver, J.A., Gonen, O., Grossman, R.I., 2005. Diffuse axonal injury in mild traumatic brain injury: a diffusion tensor imaging study. J. Neurosurg. 103, 298–303.
Irimia, A., Chambers, M.C., Torgerson, C.M., Filippou, M., Hovda, D.A., Alger, J.R., Gerig, G., Toga, A.W., Vespa, P.M., Kikinis, R., 2012. Patient-tailored connectomics visualization for the assessment of white matter atrophy in traumatic brain injury. Front. Neurol. 3, 10.
Irimia, A., Goh, S.Y., Torgerson, C.M., Chambers, M.C., Kikinis, R., Van Horn, J.D., 2013a. Forward and inverse electroencephalographic modeling in health and in acute traumatic brain injury. Clin. Neurophysiol. 124, 2129–2145.
Irimia, A., Maher, A.S., Chaudhari, N.N., Chowdhury, N.F., Jacobs, E.B., 2013b. Acute cognitive deficits after traumatic brain injury predict Alzheimer's disease-like degradation of the human default mode network. Geroscience 42, 1411–1429.
Irimia, A., Torgerson, C.M., Goh, S.Y., Van Horn, J.D., 2015. Statistical estimation of physiological brain age as a descriptor of senescence rate during adulthood. Brain Imaging Behav. 9, 678–689.
Irimia, A., Van Horn, J.D., 2015a. Epileptogenic focus localization in treatment-resistant post-traumatic epilepsy. J. Clin. Neurosci. 22, 627–631.
Irimia, A., Van Horn, J.D., 2015b. Functional neuroimaging of traumatic brain injury: advances and clinical utility. Neuropsychiatr. Dis. Treat. 11, 2355–2365.
Irimia, A., Van Horn, J.D., Vespa, P.M., 2018. Cerebral microhemorrhages due to traumatic brain injury and their effects on the aging human brain. Neurobiol. Aging 66, 158–164.
Jakola, A.S., Unsgård, G., Myrmel, K.S., Kloster, R., Torp, S.H., Losvik, O.K., Lindal, S., Solheim, O., 2013. Surgical strategy in grade II astrocytoma: a population-based analysis of survival and morbidity with a strategy of early resection as compared to watchful waiting. Acta Neurochir. (Wien) 155, 2227–2235.
Jeurissen, B., Leemans, A., Jones, D.K., Tournier, J.D., Sijbers, J., 2011. Probabilistic fiber tracking using the residual bootstrap with constrained spherical deconvolution. Hum. Brain Mapping 32, 461–479.
Jeurissen, B., Tournier, J.D., Dhollander, T., Connelly, A., Sijbers, J., 2014. Multi-tissue constrained spherical deconvolution for improved analysis of multi-shell diffusion MRI data. Neuroimage 103, 411–426.
Johansen-Berg, H., Behrens, T.E.J., 2006. Just pretty pictures? What diffusion tractography can add in clinical neuroscience. Curr. Opin. Neurol. 19, 379.
Jones, D.K., Cercignani, M., 2010. Twenty-five pitfalls in the analysis of diffusion MRI data. NMR Biomed. 23, 803–820.
Karlsgodt, K.H., van Erp, T.G., Poldrack, R.A., Bearden, C.E., Nuechterlein, K.H., Cannon, T.D., 2008. Diffusion tensor imaging of the superior longitudinal fasciculus and working memory in recent-onset schizophrenia. Biol. Psychiatry 63, 512–518.
Kawasaki, K., Matsumoto, M., Kase, M., Nagano, O., Aoyagi, K., Kageyama, T., 2017. Quantification of the radiation dose to the pyramidal tract using tractography in treatment planning for stereotactic radiosurgery. Radiol. Phys. Technol. 10, 507–514.
Kinnunen, K.M., Greenwood, R., Powell, J.H., Leech, R., Hawkins, P.C., Bonnelle, V., Patel, M.C., Counsell, S.J., Sharp, D.J., 2011. White matter damage and cognitive impairment after traumatic brain injury. Brain 134, 449–463.
Kinoshita, M., Yamada, K., Hashimoto, N., Kato, A., Izumoto, S., Baba, T., Maruno, M., Nishimura, T., Yoshimine, T., 2005. Fiber-tracking does not accurately estimate size of fiber bundle in pathological condition: initial neurosurgical experience using neuronavigation and subcortical white matter stimulation. Neuroimage 25, 424–429.
Knösche, T.R., Anwander, A., Liptrot, M., Dyrby, T.B., 2015. Validation of tractography: comparison with manganese tracing. Hum. Brain Mapping 36, 4116–4134.
Koga, T., Maruyama, K., Kamada, K., Ota, T., Shin, M., Itoh, D., Kunii, N., Ino, K., Terahara, A., Aoki, S., Masutani, Y., Saito, N., 2012. Outcomes of diffusion tensor tractography-integrated stereotactic radiosurgery. Int. J. Radiat. Oncol. Biol. Phys. 82, 799–802.
Kristo, G., Leemans, A., de Gelder, B., Raemaekers, M., Rutten, G.-J., Ramsey, N., 2013. Reliability of the corticospinal tract and arcuate fasciculus reconstructed with DTI-based tractography: implications for clinical practice. Eur. Radiol. 23, 28–36.
Kristo, G., Leemans, A., de Gelder, B., Raemaekers, M., Rutten, G.J., Ramsey, N., 2012. Reliability of the corticospinal tract and arcuate fasciculus reconstructed with DTI-based tractography: implications for clinical practice. Eur. Radiol..
Kuhnt, D., Bauer, M.H., Becker, A., Merhof, D., Zolal, A., Richter, M., Grummich, P., Ganslandt, O., Buchfelder, M., Nimsky, C., 2012. Intraoperative visualization of fiber tracking based reconstruction of language pathways in glioma surgery. Neurosurgery 70, 911–919 discussion 919-920.
Kumar, R., Gupta, R.K., Husain, M., Chaudhry, C., Srivastava, A., Saksena, S., Rathore, R.K., 2009. Comparative evaluation of corpus callosum DTI metrics in acute mild and moderate traumatic brain injury: its correlation with neuropsychometric tests. Brain Inj. 23, 675–685.
Kupper, H., Groeschel, S., Alber, M., Klose, U., Schuhmann, M.U., Wilke, M., 2015. Comparison of different tractography algorithms and validation by intraoperative stimulation in a child with a brain tumor. Neuropediatrics 46, 72–75.
Lacroix, M., Abi-Said, D., Fourney, D.R., Gokaslan, Z.L., Shi, W., DeMonte, F., Lang, F.F., McCutcheon, I.E., Hassenbusch, S.J., Holland, E., Hess, K., Michael, C., Miller, D., Sawaya, R., 2001. A multivariate analysis of 416 patients with glioblastoma multiforme: prognosis, extent of resection, and survival. J. Neurosurg. 95, 190–198.
Laitinen, T., Sierra, A., Bolkvadze, T., Pitkanen, A., Grohn, O., 2015. Diffusion tensor imaging detects chronic microstructural changes in white and gray matter after traumatic brain injury in rat. Front. Neurosci. 9, 128.
Leclercq, D., Duffau, H., Delmaire, C., Capelle, L., Gatignol, P., Ducros, M., Chiras, J., Lehéricy, S., 2010a. Comparison of diffusion tensor imaging tractography of language tracts and intraoperative subcortical stimulations. J. Neurosurg. 112, 503–511.
Leclercq, D., Duffau, H., Delmaire, C., Capelle, L., Gatignol, P., Ducros, M., Chiras, J.,

Lehéricy, S., 2010b. Comparison of diffusion tensor imaging tractography of language tracts and intraoperative subcortical stimulations. J. Neurosurg. 112, 503–511.
Li, J., Zhao, C., Rao, J.S., Yang, F.X., Wang, Z.J., Lei, J.F., Yang, Z.Y., Li, X.G., 2017. Structural and metabolic changes in the traumatically injured rat brain: high-resolution in vivo proton magnetic resonance spectroscopy at 7 T. Neuroradiology 59, 1203–1212.
Li, Y.M., Suki, D., Hess, K., Sawaya, R., 2016. The influence of maximum safe resection of glioblastoma on survival in 1229 patients: can we do better than gross-total resection? J. Neurosurg. 124, 977–988.
Lipton, M.L., Gulko, E., Zimmerman, M.E., Friedman, B.W., Kim, M., Gellella, E., Gold, T., Shifteh, K., Ardekani, B.A., Branch, C.A., 2009. Diffusion-tensor imaging implicates prefrontal axonal injury in executive function impairment following very mild traumatic brain injury. Radiology 252, 816–824.
Lo, C., Shifteh, K., Gold, T., Bello, J.A., Lipton, M.L., 2009. Diffusion tensor imaging abnormalities in patients with mild traumatic brain injury and neurocognitive impairment. J. Comput. Assist. Tomogr. 33, 293–297.
Lodygensky, G.A., West, T., Stump, M., Holtzman, D.M., Inder, T.E., Neil, J.J., 2010. In vivo MRI analysis of an inflammatory injury in the developing brain. Brain Behav. Immun. 24, 759–767.
Maier-Hein, K.H., Neher, P.F., Houde, J.C., Cote, M.A., Garyfallidis, E., Zhong, J., Chamberland, M., Yeh, F.C., Lin, Y.C., Ji, Q., Reddick, W.E., Glass, J.O., Chen, D.Q., Feng, Y., Gao, C., Wu, Y., Ma, J., He, R., Li, Q., Westin, C.F., Deslauriers-Gauthier, S., Gonzalez, J.O.O., Paquette, M., St-Jean, S., Girard, G., Rheault, F., Sidhu, J., Tax, C.M.W., Guo, F., Mesri, H.Y., David, S., Froeling, M., Heemskerk, A.M., Leemans, A., Bore, A., Pinsard, B., Bedetti, C., Desrosiers, M., Brambati, S., Doyon, J., Sarica, A., Vasta, R., Cerasa, A., Quattrone, A., Yeatman, J., Khan, A.R., Hodges, W., Alexander, S., Romascano, D., Barakovic, M., Auria, A., Esteban, O., Lemkaddem, A., Thiran, J.P., Cetingul, H.E., Odry, B.L., Mailhe, B., Nadar, M.S., Pizzagalli, F., Prasad, G., Villalon-Reina, J.E., Galvis, J., Thompson, P.M., Requejo, F.S., Laguna, P.L., Lacerda, L.M., Barrett, R., Dell'Acqua, F., Catani, M., Petit, L., Caruyer, E., Daducci, A., Dyrby, T.B., Holland-Letz, T., Hilgetag, C.C., Stieltjes, B., Descoteaux, M., 2017. The challenge of mapping the human connectome based on diffusion tractography. Nat. Commun. 8, 1349.
Makris, N., Kennedy, D.N., McInerney, S., Sorensen, A.G., Wang, R., Caviness Jr., V.S., Pandya, D.N., 2005. Segmentation of subcomponents within the superior longitudinal fascicle in humans: a quantitative, in vivo, DT-MRI study. Cereb. Cortex 15, 854–869.
Malyarenko, D.I., Ross, B.D., Chenevert, T.L., 2014. Analysis and correction of gradient nonlinearity bias in apparent diffusion coefficient measurements. Magn. Reson. Med. 71, 1312–1323.
Martino, J., Hamer, P.C.D.W., Berger, M.S., Lawton, M.T., Arnold, C.M., de Lucas, E.M., Duffau, H., 2013. Analysis of the subcomponents and cortical terminations of the perisylvian superior longitudinal fasciculus: a fiber dissection and DTI tractography study. Brain Struct. Funct. 218, 105–121.
Maruyama, K., Kamada, K., Shin, M., Itoh, D., Aoki, S., Masutani, Y., Tago, M., Kirino, T., 2005. Integration of three-dimensional corticospinal tractography into treatment planning for gamma knife surgery. J. Neurosurg. 102, 673–677.
Maruyama, K., Kamada, K., Shin, M., Itoh, D., Masutani, Y., Ino, K., Tago, M., Saito, N., 2007. Optic radiation tractography integrated into simulated treatment planning for Gamma Knife surgery. J. Neurosurg. 107, 721–726.
Maruyama, K., Koga, T., Kamada, K., Ota, T., Itoh, D., Ino, K., Igaki, H., Aoki, S., Masutani, Y., Shin, M., Saito, N., 2009. Arcuate fasciculus tractography integrated into Gamma Knife surgery. J. Neurosurg. 111, 520–526.
Mato, D., Velasquez, C., Gómez, E., Marco de Lucas, E., Martino, J., 2021. Predicting the extent of resection in low-grade glioma by using intratumoral tractography to detect eloquent fascicles within the tumor. Neurosurgery 88, E190–e202.
Maudsley, A.A., Govind, V., Levin, B., Saigal, G., Harris, L., Sheriff, S., 2015. Distributions of magnetic resonance diffusion and spectroscopy measures with traumatic brain injury. J. Neurotrauma 32, 1056–1063.
Mesri, H.Y., David, S., Viergever, M.A., Leemans, A., 2020. The adverse effect of gradient nonlinearities on diffusion MRI: from voxels to group studies. Neuroimage 205, 116127.
Miles, L., Grossman, R.I., Johnson, G., Babb, J.S., Diller, L., Inglese, M., 2008. Short-term DTI predictors of cognitive dysfunction in mild traumatic brain injury. Brain Inj. 22, 115–122.
Miller, J.A., Ding, S.L., Sunkin, S.M., Smith, K.A., Ng, L., Szafer, A., Ebbert, A., Riley, Z.L., Royall, J.J., Aiona, K., Arnold, J.M., Bennet, C., Bertagnolli, D., Brouner, K., Butler, S., Caldejon, S., Carey, A., Cuhaciyan, C., Dalley, R.A., Dee, N., Dolbeare, T.A., Facer, B.A., Feng, D., Fliss, T.P., Gee, G., Goldy, J., Gourley, L., Gregor, B.W., Gu, G., Howard, R.E., Jochim, J.M., Kuan, C.L., Lau, C., Lee, C.K., Lee, F., Lemon, T.A., Lesnar, P., McMurray, B., Mastan, N., Mosqueda, N., Naluai-Cecchini, T., Ngo, N.K., Nyhus, J., Oldre, A., Olson, E., Parente, J., Parker, P.D., Parry, S.E., Stevens, A., Pletikos, M., Reding, M., Roll, K., Sandman, D., Sarreal, M., Shapouri, S., Shapovalova, N.V., Shen, E.H., Sjoquist, N., Slaughterbeck, C.R., Smith, M., Sodt, A.J., Williams, D., Zollei, L., Fischl, B., Gerstein, M.B., Geschwind, D.H., Glass, I.A., Hawrylycz, M.J., Hevner, R.F., Huang, H., Jones, A.R., Knowles, J.A., Levitt, P., Phillips, J.W., Sestan, N., Wohnoutka, P., Dang, C., Bernard, A., Hohmann, J.G., Lein, E.S., 2014. Transcriptional landscape of the prenatal human brain. Nature 508, 199–206.
Min, Z.G., Niu, C., Rana, N., Ji, H.M., Zhang, M., 2013. Differentiation of pure vasogenic edema and tumor-infiltrated edema in patients with peritumoral edema by analyzing the relationship of axial and radial diffusivities on 3.0T MRI. Clin. Neurol. Neurosurg. 115, 1366–1370.
Mori, S., Crain, B.J., Chacko, V.P., van Zijl, P.C., 1999. Three-dimensional tracking of axonal projections in the brain by magnetic resonance imaging. Ann. Neurol. 45, 265–269.
Narayana, P.A., Yu, X., Hasan, K.M., Wilde, E.A., Levin, H.S., Hunter, J.V., Miller, E.R., Patel, V.K., Robertson, C.S., McCarthy, J.J., 2015. Multi-modal MRI of mild traumatic brain injury. Neuroimage Clin. 7, 87–97.
Neher, P.F., Descoteaux, M., Houde, J.-C., Stieltjes, B., Maier-Hein, K.H., 2015. Strengths and weaknesses of state of the art fiber tractography pipelines–a comprehensive in-vivo and phantom evaluation study using Tractometer. Med. Image Anal. 26, 287–305.
Nimsky, C., 2014. Fiber tracking–we should move beyond diffusion tensor imaging. World Neurosurg. 82, 35–36.
Nimsky, C., Ganslandt, O., Fahlbusch, R., 2006. Implementation of fiber tract navigation. Neurosurgery 58 ONS-292-303; discussion ONS-303-294.
Nimsky, C., Ganslandt, O., Hastreiter, P., Wang, R., Benner, T., Sorensen, A.G., Fahlbusch, R., 2005. Preoperative and intraoperative diffusion tensor imaging-based fiber tracking in glioma surgery. Neurosurgery 56, 130–137 discussion 138.
Norton, I., Essayed, W.I., Zhang, F., Pujol, S., Yarmarkovich, A., Golby, A.J., Kindlmann, G., Wassermann, D., Estepar, R.S.J., Rathi, Y., 2017. SlicerDMRI: open source diffusion MRI software for brain cancer research. Cancer Res. 77, e101–e103.
O'Donnell, L.J., Pasternak, O., 2014. Does diffusion MRI tell us anything about the white matter? An overview of methods and pitfalls. Schizophr. Res..
O'Donnell, L.J., Westin, C.F., 2007. Automatic tractography segmentation using a high-dimensional white matter atlas. IEEE Trans. Med. Imaging 26, 1562–1575.
O'Donnell, L.J., Suter, Y., Rigolo, L., Kahali, P., Zhang, F., Norton, I., Albi, A., Olubiyi, O., Meola, A., Essayed, W.I., 2017. Automated white matter fiber tract identification in patients with brain tumors. NeuroImage: Clinical 13, 138–153.
Ozarslan, E., Koay, C.G., Shepherd, T.M., Komlosh, M.E., Irfanoglu, M.O., Pierpaoli, C., Basser, P.J., 2013. Mean apparent propagator (MAP) MRI: a novel diffusion imaging method for mapping tissue microstructure. Neuroimage 78, 16–32.
Pantelis, E., Papadakis, N., Verigos, K., Stathochristopoulou, I., Antypas, C., Lekas, L., Tzouras, A., Georgiou, E., Salvaras, N., 2010. Integration of functional MRI and white matter tractography in stereotactic radiosurgery clinical practice. Int. J. Radiat. Oncol. Biol. Phys. 78, 257–267.
Paquette, M., Gilbert, G., M, D., 2019. Penthera 3T. Zenodo.
Park, E., McKnight, S., Ai, J., Baker, A.J., 2006. Purkinje cell vulnerability to mild and severe forebrain head trauma. J. Neuropathol. Exp. Neurol. 65, 226–234.
Parker, G.D., Marshall, A.D., Rosin, P.L., Drage, N., Richmond, S., Jones, D.K., 2013. A pitfall in the reconstruction of fibre ODFs using spherical deconvolution of diffusion MRI data. Neuroimage 65, 433–448.
Pasternak, O., Sochen, N., Gur, Y., Intrator, N., Assaf, Y., 2009. Free water elimination and mapping from diffusion MRI. Magn. Reson. Med. 62, 717–730.
Perrone, D., Aelterman, J., Pizurica, A., Jeurissen, B., Philips, W., Leemans, A., 2015. The effect of Gibbs ringing artifacts on measures derived from diffusion MRI. Neuroimage 120, 441–455.
Petrie, E.C., Cross, D.J., Yarnykh, V.L., Richards, T., Martin, N.M., Pagulayan, K., Hoff, D., Hart, K., Mayer, C., Tarabochia, M., Raskind, M.A., Minoshima, S., Peskind, E.R., 2014. Neuroimaging, behavioral, and psychological sequelae of repetitive combined blast/impact mild traumatic brain injury in Iraq and Afghanistan war veterans. J. Neurotrauma 31, 425–436.
Provenzale, J.M., McGraw, P., Mhatre, P., Guo, A.C., Delong, D., 2004. Peritumoral brain regions in gliomas and meningiomas: investigation with isotropic diffusion-weighted MR imaging and diffusion-tensor MR imaging. Radiology 232, 451–460.
Pujol, S., Wells, W., Pierpaoli, C., Brun, C., Gee, J., Cheng, G., Vemuri, B., Commowick, O., Prima, S., Stamm, A., 2015. The DTI challenge: toward standardized evaluation of diffusion tensor imaging tractography for neurosurgery. J. Neuroimaging 25, 875–882.
Qazi, A.A., Radmanesh, A., O'Donnell, L., Kindlmann, G., Peled, S., Whalen, S., Westin, C.F., Golby, A.J., 2009. Resolving crossings in the corticospinal tract by two-tensor streamline tractography: Method and clinical assessment using fMRI. Neuroimage 47 (2), T98–106 Suppl.
Radmanesh, A., Zamani, A.A., Whalen, S., Tie, Y., Suarez, R.O., Golby, A.J., 2015. Comparison of seeding methods for visualization of the corticospinal tracts using single tensor tractography. Clinical neurology and neurosurgery 129, 44–49.
Rahman, M., Abbatematteo, J., De Leo, E.K., Kubilis, P.S., Vaziri, S., Bova, F., Sayour, E., Mitchell, D., Quinones-Hinojosa, A., 2017. The effects of new or worsened postoperative neurological deficits on survival of patients with glioblastoma. J. Neurosurg. 127, 123–131.
Reese, T.G., Heid, O., Weisskoff, R.M., Wedeen, V.J., 2003. Reduction of eddy-current-induced distortion in diffusion MRI using a twice-refocused spin echo. Magn. Reson. Med. 49, 177–182.
Reveley, C., Seth, A.K., Pierpaoli, C., Silva, A.C., Yu, D., Saunders, R.C., Leopold, D.A., Ye, F.Q., 2015. Superficial white matter fiber systems impede detection of long-range cortical connections in diffusion MR tractography. Proc. Natl. Acad. Sci. U. S. A. 112, E2820–E2828.
Rheault, F., St-Onge, E., Sidhu, J., Maier-Hein, K., Tzourio-Mazoyer, N., Petit, L., Descoteaux, M., 2019. Bundle-specific tractography with incorporated anatomical and orientational priors. Neuroimage 186, 382–398.
Rilling, J.K., Glasser, M.F., Preuss, T.M., Ma, X., Zhao, T., Hu, X., Behrens, T.E., 2008. The evolution of the arcuate fasciculus revealed with comparative DTI. Nat. Neurosci. 11, 426–428.
Rokem, A., Yeatman, J.D., Pestilli, F., Kay, K.N., Mezer, A., van der Walt, S., Wandell, B.A., 2015. Evaluating the accuracy of diffusion MRI models in white matter. PLoS One 10, e0123272.
Rostowsky, K.A., Maher, A.S., Irimia, A., 2018. Macroscale white matter alterations due to traumatic cerebral microhemorrhages are revealed by diffusion tensor imaging. Front. Neurol. 9.
Salo, R.A., Belevich, I., Manninen, E., Jokitalo, E., Grohn, O., Sierra, A., 2018. Quantification of anisotropy and orientation in 3D electron microscopy and diffusion tensor imaging in injured rat brain. Neuroimage 172, 404–414.
Sanchez-Catasus, C.A., Bohnen, N.I., Yeh, F.C., D'Cruz, N., Kanel, P., Muller, M., 2020.

Dopaminergic nigrostriatal connectivity in early Parkinson disease: in vivo neuroimaging study of (11)C-DTBZ PET combined with correlational tractography. J. Nucl. Med..
Sanvito, F., Caverzasi, E., Riva, M., Jordan, K.M., Blasi, V., Scifo, P., Iadanza, A., Crespi, S.A., Cirillo, S., Casarotti, A., Leonetti, A., Puglisi, G., Grimaldi, M., Bello, L., Gorno-Tempini, M.L., Henry, R.G., Falini, A., Castellano, A., 2020. fMRI-Targeted High-Angular Resolution Diffusion MR Tractography to Identify Functional Language Tracts in Healthy Controls and Glioma Patients. Front. Neurosci. 14, 225.
Saur, D., Kreher, B.W., Schnell, S., Kummerer, D., Kellmeyer, P., Vry, M.S., Umarova, R., Musso, M., Glauche, V., Abel, S., Huber, W., Rijntjes, M., Hennig, J., Weiller, C., 2008. Ventral and dorsal pathways for language. Proc. Natl. Acad. Sci. U. S. A. 105, 18035–18040.
Schilling, K., Gao, Y., Janve, V., Stepniewska, I., Landman, B.A., Anderson, A.W., 2018a. Confirmation of a gyral bias in diffusion MRI fiber tractography. Hum. Brain Mapp. 39, 1449–1466.
Schilling, K., Janve, V., Gao, Y., Stepniewska, I., Landman, B.A., Anderson, A.W., 2016. Comparison of 3D orientation distribution functions measured with confocal microscopy and diffusion MRI. Neuroimage 129, 185–197.
Schilling, K.G., Gao, Y., Stepniewska, I., Janve, V., Landman, B.A., Anderson, A.W., 2019a. Histologically derived fiber response functions for diffusion MRI vary across white matter fibers-An ex vivo validation study in the squirrel monkey brain. NMR Biomed. 32, e4090.
Schilling, K.G., Janve, V., Gao, Y., Stepniewska, I., Landman, B.A., Anderson, A.W., 2018b. Histological validation of diffusion MRI fiber orientation distributions and dispersion. Neuroimage 165, 200–221.
Schilling, K.G., Nath, V., Hansen, C., Parvathaneni, P., Blaber, J., Gao, Y., Neher, P., Aydogan, D.B., Shi, Y., Ocampo-Pineda, M., 2019b. Limits to anatomical accuracy of diffusion tractography using modern approaches. Neuroimage 185, 1–11.
Schilling, K.G., Petit, L., Rheault, F., Remedios, S., Pierpaoli, C., Anderson, A.W., Landman, B.A., Descoteaux, M., 2020. Brain connections derived from diffusion MRI tractography can be highly anatomically accurate—if we know where white matter pathways start, where they end, and where they do not go. Brain Struct. Funct. 225, 2387–2402.
Schilling, K.G., Rheault, F., Petit, L., Hansen, C.B., Nath, V., Yeh, F.-C., Girard, G., Barakovic, M., Rafael-Patino, J., Yu, T., 2021. Tractography dissection variability: what happens when 42 groups dissect 14 white matter bundles on the same dataset? bioRxiv 2020.2010. 2007.321083.
Schmahmann, J.D., Pandya, D.N., Wang, R., Dai, G., D'Arceuil, H.E., de Crespigny, A.J., Wedeen, V.J., 2007. Association fibre pathways of the brain: parallel observations from diffusion spectrum imaging and autoradiography. Brain 130, 630–653.
Schonberg, T., Pianka, P., Hendler, T., Pasternak, O., Assaf, Y., 2006. Characterization of displaced white matter by brain tumors using combined DTI and fMRI. Neuroimage 30, 1100–1111.
Sclocco, R., Beissner, F., Bianciardi, M., Polimeni, J.R., Napadow, V., 2018. Challenges and opportunities for brainstem neuroimaging with ultrahigh field MRI. Neuroimage 168, 412–426.
Setsompop, K., Cohen-Adad, J., Gagoski, B.A., Raij, T., Yendiki, A., Keil, B., Wedeen, V.J., Wald, L.L., 2012a. Improving diffusion MRI using simultaneous multi-slice echo planar imaging. Neuroimage 63, 569–580.
Setsompop, K., Gagoski, B.A., Polimeni, J.R., Witzel, T., Wedeen, V.J., Wald, L.L., 2012b. Blipped-controlled aliasing in parallel imaging for simultaneous multislice echo planar imaging with reduced g-factor penalty. Magn. Reson. Med. 67, 1210–1224.
Smith, R.E., Tournier, J.D., Calamante, F., Connelly, A., 2012. Anatomically-constrained tractography: improved diffusion MRI streamlines tractography through effective use of anatomical information. Neuroimage 62, 1924–1938.
Smith, R.E., Tournier, J.D., Calamante, F., Connelly, A., 2013. SIFT: Spherical-deconvolution informed filtering of tractograms. Neuroimage 67, 298–312.
Smits, M., Vernooij, M.W., Wielopolski, P.A., Vincent, A.J., Houston, G.C., van der Lugt, A., 2007. Incorporating functional MR imaging into diffusion tensor tractography in the preoperative assessment of the corticospinal tract in patients with brain tumors. AJNR Am. J. Neuroradiol. 28, 1354–1361.
Song, S.K., Sun, S.W., Ju, W.K., Lin, S.J., Cross, A.H., Neufeld, A.H., 2003. Diffusion tensor imaging detects and differentiates axon and myelin degeneration in mouse optic nerve after retinal ischemia. Neuroimage 20, 1714–1722.
Song, S.K., Sun, S.W., Ramsbottom, M.J., Chang, C., Russell, J., Cross, A.H., 2002. Dysmyelination revealed through MRI as increased radial (but unchanged axial) diffusion of water. Neuroimage 17, 1429–1436.
Song, S.K., Yoshino, J., Le, T.Q., Lin, S.J., Sun, S.W., Cross, A.H., Armstrong, R.C., 2005. Demyelination increases radial diffusivity in corpus callosum of mouse brain. Neuroimage 26, 132–140.
Sosnovik, D.E., Wang, R., Dai, G., Reese, T.G., Wedeen, V.J., 2009. Diffusion MR tractography of the heart. J. Cardiovasc. Magn. Resonance 11, 1–15.
Spanos, G., Wilde, E., Bigler, E., Cleavinger, H., Fearing, M., Levin, H., Li, X., Hunter, J., 2007. Cerebellar atrophy after moderate-to-severe pediatric traumatic brain injury. Am. J. Neuroradiol. 28, 537–542.
Sporns, O., Tononi, G., Kotter, R., 2005. The human connectome: a structural description of the human brain. PLoS Comput. Biol. 1, e42.
Stejskal, E.O., Tanner, J.E., 1965. Spin Diffusion Measurements: spin Echoes in the Presence of a Time-Dependent Field Gradient. J. Chem. Phys. 42, 288–292.
Sullivan, S., Eucker, S.A., Gabrieli, D., Bradfield, C., Coats, B., Maltese, M.R., Lee, J., Smith, C., Margulies, S.S., 2015. White matter tract-oriented deformation predicts traumatic axonal brain injury and reveals rotational direction-specific vulnerabilities. Biomech. Model. Mechanobiol. 14, 877–896.
Sun, S.W., Liang, H.F., Trinkaus, K., Cross, A.H., Armstrong, R.C., Song, S.K., 2006. Noninvasive detection of cuprizone induced axonal damage and demyelination in the mouse corpus callosum. Magn. Reson. Med. 55, 302–308.
Tan, E.T., Marinelli, L., Slavens, Z.W., King, K.F., Hardy, C.J., 2013. Improved correction for gradient nonlinearity effects in diffusion-weighted imaging. J. Magn. Reson. Imaging 38, 448–453.
Thomas, C., Ye, F.Q., Irfanoglu, M.O., Modi, P., Saleem, K.S., Leopold, D.A., Pierpaoli, C., 2014. Anatomical accuracy of brain connections derived from diffusion MRI tractography is inherently limited. Proc. Natl. Acad. Sci. U. S. A. 111, 16574–16579.
Tong, Q., He, H., Gong, T., Li, C., Liang, P., Qian, T., Sun, Y., Ding, Q., Li, K., Zhong, J., 2020. Multicenter dataset of multi-shell diffusion MRI in healthy traveling adults with identical settings. Sci. Data 7, 157.
Toth, A., Kovacs, N., Perlaki, G., Orsi, G., Aradi, M., Komaromy, H., Ezer, E., Bukovics, P., Farkas, O., Janszky, J., Doczi, T., Buki, A., Schwarcz, A., 2013. Multi-modal magnetic resonance imaging in the acute and sub-acute phase of mild traumatic brain injury: can we see the difference? J. Neurotrauma 30, 2–10.
Tournier, J.D., Calamante, F., Connelly, A., 2007. Robust determination of the fibre orientation distribution in diffusion MRI: non-negativity constrained super-resolved spherical deconvolution. Neuroimage 35, 1459–1472.
Tournier, J.D., Calamante, F., Gadian, D.G., Connelly, A., 2004. Direct estimation of the fiber orientation density function from diffusion-weighted MRI data using spherical deconvolution. Neuroimage 23, 1176–1185.
Tournier, J.D., Mori, S., Leemans, A., 2011. Diffusion tensor imaging and beyond. Magn. Reson. Med. 65, 1532–1556.
Tournier, J.D., Smith, R., Raffelt, D., Tabbara, R., Dhollander, T., Pietsch, M., Christiaens, D., Jeurissen, B., Yeh, C.H., Connelly, A., 2019. MRtrix3: a fast, flexible and open software framework for medical image processing and visualisation. Neuroimage 202, 116137.
Tournier, J.D., Yeh, C.H., Calamante, F., Cho, K.H., Connelly, A., Lin, C.P., 2008. Resolving crossing fibres using constrained spherical deconvolution: validation using diffusion-weighted imaging phantom data. Neuroimage 42, 617–625.
Tremblay, S., Henry, L.C., Bedetti, C., Larson-Dupuis, C., Gagnon, J.F., Evans, A.C., Theoret, H., Lassonde, M., De Beaumont, L., 2014. Diffuse white matter tract abnormalities in clinically normal ageing retired athletes with a history of sports-related concussions. Brain 137, 2997–3011.
Trotter, B.B., Robinson, M.E., Milberg, W.P., McGlinchey, R.E., Salat, D.H., 2015. Military blast exposure, ageing and white matter integrity. Brain 138, 2278–2292.
Tuch, D.S., 2004. Q-ball imaging. Magn. Reson. Med. 52, 1358–1372.
Tuch, D.S., Reese, T.G., Wiegell, M.R., Makris, N., Belliveau, J.W., Wedeen, V.J., 2002. High angular resolution diffusion imaging reveals intravoxel white matter fiber heterogeneity. Magn. Reson. Med. 48, 577–582.
Tuncer, M.S., Salvati, L.F., Grittner, U., Hardt, J., Schilling, R., Bahrend, I., Silva, L.L., Fekonja, L.S., Faust, K., Vajkoczy, P., Rosenstock, T., Picht, T., 2021. Towards a tractography-based risk stratification model for language area associated gliomas. Neuroimage Clin. 29, 102541.
Van Essen, D.C., Ugurbil, K., Auerbach, E., Barch, D., Behrens, T.E., Bucholz, R., Chang, A., Chen, L., Corbetta, M., Curtiss, S.W., Della Penna, S., Feinberg, D., Glasser, M.F., Harel, N., Heath, A.C., Larson-Prior, L., Marcus, D., Michalareas, G., Moeller, S., Oostenveld, R., Petersen, S.E., Prior, F., Schlaggar, B.L., Smith, S.M., Snyder, A.Z., Xu, J., Yacoub, E., 2012. The Human Connectome Project: a data acquisition perspective. Neuroimage 62, 2222–2231.
Van Horn, J.D., Bhattrai, A., Irimia, A., 2017. Multimodal imaging of neurometabolic pathology due to traumatic brain injury. Trends Neurosci. 40, 39–59.
Vanderweyen, D.C., Theaud, G., Sidhu, J., Rheault, F., Sarubbo, S., Descoteaux, M., Fortin, D., 2020. The role of diffusion tractography in refining glial tumor resection. Brain Struct. Funct..
Vanegas-Arroyave, N., Lauro, P.M., Huang, L., Hallett, M., Horovitz, S.G., Zaghloul, K.A., Lungu, C., 2016. Tractography patterns of subthalamic nucleus deep brain stimulation. Brain 139, 1200–1210.
Veraart, J., Fieremans, E., Jelescu, I.O., Knoll, F., Novikov, D.S., 2016. Gibbs ringing in diffusion MRI. Magn. Reson. Med. 76, 301–314.
Vos, S.B., Tax, C.M., Luijten, P.R., Ourselin, S., Leemans, A., Froeling, M., 2017. The importance of correcting for signal drift in diffusion MRI. Magn. Reson. Med. 77, 285–299.
Wang, Y., Wang, Q., Haldar, J.P., Yeh, F.C., Xie, M., Sun, P., Tu, T.W., Trinkaus, K., Klein, R.S., Cross, A.H., Song, S.K., 2011. Quantification of increased cellularity during inflammatory demyelination. Brain 134, 3590–3601.
Warrington, S., Bryant, K.L., Khrapitchev, A.A., Sallet, J., Charquero-Ballester, M., Douaud, G., Jbabdi, S., Mars, R.B., Sotiropoulos, S.N., 2020. XTRACT - Standardised protocols for automated tractography in the human and macaque brain. Neuroimage 217, 116923.
Wassermann, D., Makris, N., Rathi, Y., Shenton, M., Kikinis, R., Kubicki, M., Westin, C.F., 2016. The white matter query language: a novel approach for describing human white matter anatomy. Brain Struct. Funct..
Wasserthal, J., Neher, P., Maier-Hein, K.H., 2018. TractSeg - fast and accurate white matter tract segmentation. Neuroimage 183, 239–253.
Wedeen, V.J., Hagmann, P., Tseng, W.Y., Reese, T.G., Weisskoff, R.M., 2005. Mapping complex tissue architecture with diffusion spectrum magnetic resonance imaging. Magn. Reson. Med. 54, 1377–1386.
Wedeen, V.J., Rosene, D.L., Wang, R., Dai, G., Mortazavi, F., Hagmann, P., Kaas, J.H., Tseng, W.Y., 2012. The geometric structure of the brain fiber pathways. Science 335, 1628–1634.
Wilkins, B., Lee, N., Gajawelli, N., Law, M., Lepore, N., 2015a. Fiber estimation and tractography in diffusion MRI: development of simulated brain images and comparison of multi-fiber analysis methods at clinical b-values. Neuroimage 109, 341–356.
Wilkins, B., Lee, N., Gajawelli, N., Law, M., Leporé, N., 2015b. Fiber estimation and tractography in diffusion MRI: development of simulated brain images and comparison of multi-fiber analysis methods at clinical b-values. Neuroimage 109, 341–356.
Winklewski, P.J., Sabisz, A., Naumczyk, P., Jodzio, K., Szurowska, E., Szarmach, A., 2018.

Understanding the physiopathology behind axial and radial diffusivity changes-what do we know? Front. Neurol. 9, 92.
Witwer, B.P., Moftakhar, R., Hasan, K.M., Deshmukh, P., Haughton, V., Field, A., Arfanakis, K., Noyes, J., Moritz, C.H., Meyerand, M.E., Rowley, H.A., Alexander, A.L., Badie, B., 2002. Diffusion-tensor imaging of white matter tracts in patients with cerebral neoplasm. J. Neurosurg. 97, 568–575.
Wooten, D.W., Ortiz-Teran, L., Zubcevik, N., Zhang, X., Huang, C., Sepulcre, J., Atassi, N., Johnson, K.A., Zafonte, R.D., El Fakhri, G., 2019. Multi-modal signatures of tau pathology, neuronal fiber integrity, and functional connectivity in traumatic brain injury. J. Neurotrauma 36, 3233–3243.
Wright, D.K., Johnston, L.A., Kershaw, J., Ordidge, R., O'Brien, T.J., Shultz, S.R., 2017. Changes in apparent fiber density and track-weighted imaging metrics in white matter following experimental traumatic brain injury. J. Neurotrauma 34, 2109–2118.
Wright, D.K., Trezise, J., Kamnaksh, A., Bekdash, R., Johnston, L.A., Ordidge, R., Semple, B.D., Gardner, A.J., Stanwell, P., O'Brien, T.J., Agoston, D.V., Shultz, S.R., 2016. Behavioral, blood, and magnetic resonance imaging biomarkers of experimental mild traumatic brain injury. Sci. Rep. 6, 28713.
Wu, J.S., Zhou, L.F., Tang, W.J., Mao, Y., Hu, J., Song, Y.Y., Hong, X.N., Du, G.H., 2007. Clinical evaluation and follow-up outcome of diffusion tensor imaging-based functional neuronavigation: a prospective, controlled study in patients with gliomas involving pyramidal tracts. Neurosurgery 61, 935–948 discussion 948-939.
Wu, W., Miller, K.L., 2017. Image formation in diffusion MRI: a review of recent technical developments. J. Magn. Reson. Imaging 46, 646–662.
Wu, Y.C., Alexander, A.L., 2007. Hybrid diffusion imaging. Neuroimage 36, 617–629.
Wu, Y.C., Mustafi, S.M., Harezlak, J., Kodiweera, C., Flashman, L.A., McAllister, T.W., 2018. Hybrid Diffusion Imaging in Mild Traumatic Brain Injury. J. Neurotrauma 35, 2377–2390.
Xie, M., Tobin, J.E., Budde, M.D., Chen, C.I., Trinkaus, K., Cross, A.H., McDaniel, D.P., Song, S.K., Armstrong, R.C., 2010. Rostrocaudal analysis of corpus callosum demyelination and axon damage across disease stages refines diffusion tensor imaging correlations with pathological features. J. Neuropathol. Exp. Neurol. 69, 704–716.
Yang, G., McNab, J.A., 2019. Eddy current nulled constrained optimization of isotropic diffusion encoding gradient waveforms. Magn. Reson. Med. 81, 1818–1832.
Yang, J., Li, Q., Wang, Z., Qi, C., Han, X., Lan, X., Wan, J., Wang, W., Zhao, X., Hou, Z., Gao, C., Carhuapoma, J.R., Mori, S., Zhang, J., Wang, J., 2017. Multimodality MRI assessment of grey and white matter injury and blood-brain barrier disruption after intracerebral haemorrhage in mice. Sci. Rep. 7, 40358.
Yeatman, J.D., Dougherty, R.F., Myall, N.J., Wandell, B.A., Feldman, H.M., 2012. Tract profiles of white matter properties: automating fiber-tract quantification. PLoS One 7, e49790.
Yeh, F.C., 2020. Shape analysis of the human association pathways. Neuroimage 223, 117329.
Yeh, F.C., Badre, D., Verstynen, T., 2016. Connectometry: a statistical approach harnessing the analytical potential of the local connectome. Neuroimage 125, 162–171.
Yeh, F.C., Liu, L., Hitchens, T.K., Wu, Y.L., 2017. Mapping immune cell infiltration using restricted diffusion MRI. Magn. Reson. Med. 77, 603–612.
Yeh, F.C., Panesar, S., Fernandes, D., Meola, A., Yoshino, M., Fernandez-Miranda, J.C., Vettel, J.M., Verstynen, T., 2018. Population-averaged atlas of the macroscale human structural connectome and its network topology. Neuroimage 178, 57–68.
Yeh, F.C., Verstynen, T.D., Wang, Y., Fernandez-Miranda, J.C., Tseng, W.Y., 2013. Deterministic diffusion fiber tracking improved by quantitative anisotropy. PLoS One 8, e80713.
Yeh, F.C., Wedeen, V.J., Tseng, W.Y., 2010. Generalized q-sampling imaging. IEEE Trans. Med. Imaging 29, 1626–1635.
Yeh, F.C., Zaydan, I.M., Suski, V.R., Lacomis, D., Richardson, R.M., Maroon, J.C., Barrios–Martinez, J., 2019. Differential tractography as a track-based biomarker for neuronal injury. Neuroimage 202, 116131.
Yendiki, A., Panneck, P., Srinivasan, P., Stevens, A., Zollei, L., Augustinack, J., Wang, R., Salat, D., Ehrlich, S., Behrens, T., Jbabdi, S., Gollub, R., Fischl, B., 2011. Automated probabilistic reconstruction of white-matter pathways in health and disease using an atlas of the underlying anatomy. Front. Neuroinform. 5, 23.
Young, R.J., Knopp, E.A., 2006. Brain MRI: tumor evaluation. J. Magn. Resonance Imaging 24, 709–724.
Yuh, E.L., Cooper, S.R., Mukherjee, P., Yue, J.K., Lingsma, H.F., Gordon, W.A., Valadka, A.B., Okonkwo, D.O., Schnyer, D.M., Vassar, M.J., Maas, A.I., Manley, G.T., Track-Tbi, I., 2014. Diffusion tensor imaging for outcome prediction in mild traumatic brain injury: a TRACK-TBI study. J. Neurotrauma 31, 1457–1477.
Zhang, H., Schneider, T., Wheeler-Kingshott, C.A., Alexander, D.C., 2012. NODDI: practical in vivo neurite orientation dispersion and density imaging of the human brain. Neuroimage 61, 1000–1016.
Zhang, H., Wang, Y., Lu, T., Qiu, B., Tang, Y., Ou, S., Tie, X., Sun, C., Xu, K., Wang, Y., 2013. Differences between generalized q-sampling imaging and diffusion tensor imaging in the preoperative visualization of the nerve fiber tracts within peritumoral edema in brain. Neurosurgery 73, 1044–1053 discussion 1053.
Zhao, W., Cai, Y., Li, Z., Ji, S., 2017. Injury prediction and vulnerability assessment using strain and susceptibility measures of the deep white matter. Biomech. Model. Mechanobiol. 16, 1709–1727.
Zhu, F.P., Wu, J.S., Song, Y.Y., Yao, C.J., Zhuang, D.X., Xu, G., Tang, W.J., Qin, Z.Y., Mao, Y., Zhou, L.F., 2012. Clinical application of motor pathway mapping using diffusion tensor imaging tractography and intraoperative direct subcortical stimulation in cerebral glioma surgery: a prospective cohort study. Neurosurgery 71, 1170–1183 discussion 1183-1174.
Ziegler, E., Rouillard, M., Andre, E., Coolen, T., Stender, J., Balteau, E., Phillips, C., Garraux, G., 2014. Mapping track density changes in nigrostriatal and extranigral pathways in Parkinson's disease. Neuroimage 99, 498–508.
Zolal, A., Hejčl, A., Vachata, P., Bartoš, R., Humhej, I., Malucelli, A., Nováková, M., Hrach, K., Derner, M., Sameš, M., 2012. The use of diffusion tensor images of the corticospinal tract in intrinsic brain tumor surgery: a comparison with direct subcortical stimulation. Neurosurgery 71, 331–340 discussion 340.
Zollei, L., Jaimes, C., Saliba, E., Grant, P.E., Yendiki, A., 2019. TRActs constrained by UnderLying INfant anatomy (TRACULInA): an automated probabilistic tractography tool with anatomical priors for use in the newborn brain. Neuroimage 199, 1–17.